Sedimentary Geology 452 (2023) 106422

Contents lists available at ScienceDirect

Sedimentary Geology

journal homepage: www.elsevier.com/locate/sedgeo

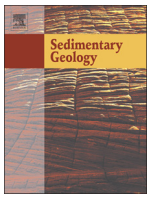

Going with the flow: Sedimentary processes along karst conduits within Chalk aquifers, northern France

Daniel Ballesteros [a,b,*], Andrew Farrant [c], Diana Sahy [c], Kim Genuite [a], Ingrid Bejarano [a], Carole Nehme [a]

[a] UMR 6266 IDEES, University of Rouen Normandy/CNRS, Mont St-Aignan CEDEX, France
[b] Department of Geodynamics, University of Granada, Campus de Fuentenueva s/n, 18071 Granada, Spain
[c] British Geological Survey, Keyworth, Nottingham NG12 5GG, United Kingdom

ARTICLE INFO

Article history:
Received 15 March 2023
Received in revised form 8 May 2023
Accepted 9 May 2023
Available online 18 May 2023

Editor: Dr. Catherine Chagué

Keywords:
Aquifer
Cave
Chalk
Karst
Sediment
Sedimentology

ABSTRACT

Sediment-filled caves, conduits and voids are common in many karst regions. These voids and the sediment they contain are important palaeoclimatic and palaeoenvironmental archives, but often have an adverse impact on engineering projects, mineral extraction and hydrogeology. Most studies into fluvial sedimentation in karst aquifers have focussed on more traditional karst areas. However, the nature and extent of fluvial sedimentation within caves and conduits in the important Upper Cretaceous Chalk Group aquifer (NW and Central Europe), and their impacts are less well known. This is principally due to a lack of accessible Chalk caves with exposed 3D sediment archives for study. Fortunately, the discovery of the World's longest Chalk cave system by underground quarrying at Caumont in the Seine valley near Rouen, northern France, has exposed numerous sediment sections along 2.4 km of passage. Detailed analysis of the stratigraphy, mineralogy, sedimentology, provenance and the chronology of the exposed sediments including the novel use of Gamma-ray spectrometry, reveals complex stratigraphy and lateral facies distribution along a karst conduit. The depositional model comprises five allostratigraphical units since the mid-Chibanian, separated by periods of erosion. The units are derived from hyper-concentrated and sediment-laden flows, and include thalweg, channel, slackwater, backswamp speleothem facies and debris flow deposits that are interbedded. Speleothems precipitated during MIS 7, 6, 5e and 1. During MIS 7–6, detrital sediments filled almost all Chalk conduits, similar to other caves in the European Atlantic Margin, coevally with the Penultima (Saalian) Glacial Cycle and a maximum of the Earth eccentricity. Detrital sediments are derived from the erosion of local Chalk bedrocks as well as metamorphic and igneous rocks of remote areas, such as Morvan massif and Massif Central. The depositional model is consistent with the conception of the Chalk as a karst aquifer. Significant sediment aggradation caused upwards dissolution (paragenesis), conduit occlusion and subsequent genesis of new conduits by flow diversion, potentially altering the functioning of the chalk aquifer and the interpretation of Chalk hydrogeology (e.g., dye-tracing tests).

1. Introduction

Many caves, conduits and dissolution pipes are infilled with detrital sediment (White, 2007). These sediment-filled cavities have significant impacts on engineering projects, mineral abstraction and groundwater flow in carbonate aquifers (Bouchaou et al., 2002; Herman et al., 2008, 2012; Murphy et al., 2008). Engineering effects include reduced rock mass quality, hazards for drilling, tunnelling, structural foundations, slope stability, and sinkhole formation (Culshaw and Waltham, 1987; Waltham and Fookes, 2003; Warren and Mortimore, 2003; Edmonds, 2008). Sediment-filled cavities pose issues for quarry and mine management, resource loss and potential geohazards (Lolcama et al., 2002). Detrimental hydrogeological effects include the occlusion of conduits by sediment impacting groundwater flow (Bettel et al., 2022), increased water turbidity (Fournier et al., 2007), potential transport mechanisms for bacteria (Mahler et al., 2000) and heavy metals (Vesper et al., 2001), and reduced efficacy of artificial tracers (Schiperski et al., 2016). Cave sediments are also potential important archaeological, palaeoenvironmental and palaeoclimatic archives (Goldberg and Sherwood, 2006; Lundberg and McFarlane, 2007; González-Lemos et al., 2014). For all these reasons, various studies have examined how detrital sediment infills within caves and conduits can influence the aquifer functioning and spring discharge (Veni, 2013), including Chalk aquifers (Massei et al., 2003).

* Corresponding author at: Department of Geodynamics, University of Granada, Campus de Fuentenueva s/n, 18071 Granada, Spain.
E-mail addresses: dballesteros@ugr.es (D. Ballesteros), arf@bgs.ac.uk (A. Farrant), dihy@bgs.ac.uk (D. Sahy), ingrid.bejarano-arias@univ-rouen.fr (I. Bejarano), carole.nehme@univ-rouen.fr (C. Nehme).

https://doi.org/10.1016/j.sedgeo.2023.106422

Sediment-filled dissolution pipes, conduits and cavities are common in the Upper Cretaceous Chalk Group. The Chalk forms the principal aquifer in NW and N Central Europe (Fig. 1a) which provides >60 % of the public water supply (Crampon et al., 1993; Price et al., 1993) and maintains important wetlands and stream habitats (House et al., 2016; Wetherell, 2023). The Chalk also underlies densely populated areas and presents significant variability in engineering properties and geotechnical behaviour (Waltham and Fookes, 2003; Mortimore et al., 2011). Similar Chalk-type aquifers occur around the globe, for instance, the Edwards aquifer in Texas (Sharp et al., 2019), the North Coast Aquifer System in Puerto Rico (Ghasemizadeh et al., 2008) and the Nullabor Plain in Australia (Miller et al., 2012).

The aquifer properties of the Chalk derive from its particular lithology: a soft coccolith biomicrite with high primary porosity (20–40 %) and low primary permeability, but often significant transmissivity through fractures and karstic conduits (El Janyani et al., 2012; Descamps et al., 2017), many of which contain detrital sediment fills. This makes predicting groundwater flow through the Chalk a major challenge (Foley and Worthington, 2023). The Chalk has been classically conceived as a dual-porosity aquifer (Hakoun et al., 2017) with local or negligible karstification (Roux et al., 2019). Increasingly, recent studies conceived the Chalk as a triple porosity karst aquifer due to hydrogeological functioning (high transmissivity and hydraulic conductivity) and widespread occurrence of karst features such as dolines, sinking streams, large springs, dissolution pipes and caves and conduits often developed by mixing dissolution (for further details see Maurice et al., 2023).

Most Chalk conduits are too small to enter, have no surface connection or are water/sediment filled making direct observations very difficult. Therefore, the study of detrital sediment infills within karst features is usually restricted to quarry and cliff sections (Dobrowolski et al., 2012; Grube et al., 2017), temporary exposures during construction, and downhole imagery from boreholes (Maurice et al., 2012). These typically offer 2D snapshots, but do not permit detailed investigation of stratigraphical correlations and lateral facies variations. For these reasons, there are very few sedimentological studies of cave sediments in the Chalk (Rodet et al., 2006) compared to classical limestone caves (e.g., Murszewski et al., 2020; Kurečić et al., 2021). The few studies that have been carried out in Chalk caves focused on the granulometry, chemical composition, clay minerology and provenance of detrital sediments (Laignel et al., 2004; Chédeville et al., 2015). Chronological data is only available in two significant cases, based on palaeomagnetism and U-series dating (Nehme et al., 2020), and thermoluminescence on sediments in epikarst cavities (Dobrowolski and Fedorowicz, 2007; Dobrowolski and Mroczek, 2015). However, sedimentary facies, model deposition and lateral variability within Chalk conduits remain poorly understood.

The longest known Chalk cave is the 4.2 km long Caumont cave system in the lower Seine valley (Fig. 1b). This was discovered by extensive underground quarrying in the 13th century (Ballesteros et al., 2022a).

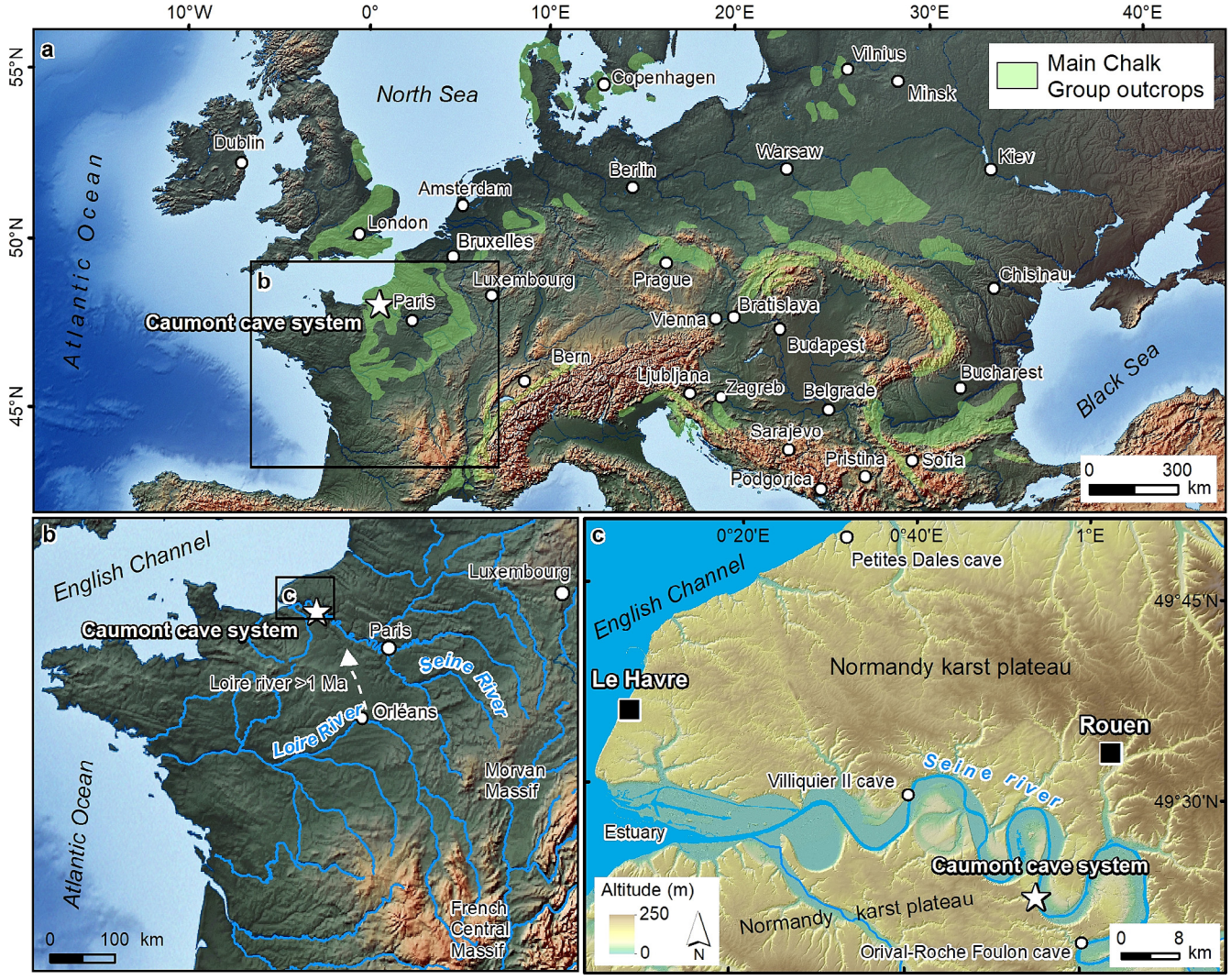

Fig. 1. (a) Chalk areas along West-Central Europe. (b) Location of Seine and Loire rivers in France; a white arrow indicates the position of the River Loire towards the River Seine near Orléans prior to 1 Ma (Tourenq and Pomerol, 1995). (c) Location of Caumont cave system in the lower Seine valley, which here is incised >100 m into the Normandy karst plateau.

The karstic conduits intersected by this quarry host detrital sediments and speleothems that can be related to the incision of the River Seine (Nehme et al., 2020) and the wider landscape evolution during the Quaternary (Antoine et al., 2003; Westaway, 2004). Numerous stratigraphical sections throughout the conduit network facilitate a comprehensive three-dimensional study of the cave sediments and facies associations. We focused on determining the nature, facies distribution, mineralogy, depositional processes, chronology and provenance of the detrital sediments within the Caumont cave system to understanding the impact of clastic sedimentation on groundwater systems elsewhere in the Chalk aquifer. For that, the first depositional model of a Chalk cave was carried out providing new insights into the sedimentology of Chalk cave infills and methodological study.

2. Setting

The cave system intersected by the Caumont quarries (49°22′41″N, 0°54′47″E) is located on the south side of the Seine valley (Fig. 1b-c), which is incised >100 m into the Normandy karst plateau (northern France). The karst plateau is mainly formed by the Upper Cretaceous Chalk Group, comprising 300 m of flint-rich coccolithic limestone (Lasseur et al., 2009; Mortimore, 2019).

The present River Seine has a fluvial basin of ca. 76,000 km^2 (Fig. 1b). During the Pliocene to early Quaternary, the catchment extended further south, encompassing the current upper Loire catchment (Tourenq and Pomerol, 1995; Westaway, 2004). Pliocene fluvio-marine deposits (e.g., the St-Eustache Sand Formation) indicated that marine transgressions affected the Seine-Loire basin up to late Pliocene (Dugué et al., 2009). Subsequently, the River Seine has incised at rate of 0.05–0.3 mm·ka^{-1}, based on magnetostratigraphy from cave sediments over the last 1.2 Ma (Nehme et al., 2020). During this time, the River Seine developed large free and semi-entrenched (ingrown) meanders (Fig. 1c) (Genuite et al., 2021) and fluvial terraces (Lautridou et al., 1999; Antoine et al., 2000, 2007). Coevally, the karstification has created branchwork and maze caves (Rodet, 2013), typically associated with inception horizons on low permeability beds (hardgrounds, marls and sheet flints) within the Chalk (Ballesteros et al., 2020; Farrant et al., 2023). At present >8 km of cave passage has been explored. Many of these are multilevel and have a complex history (Rodet and Lautridou, 2003), characterised by phreatic/epiphreatic and paragenetic conduits (sensu; Farrant and Smart, 2011), sometimes entrenched by vadose water and often filled by quartz-rich detrital sediments and occasional speleothems, some of which have been dated to 570 ± 52 ka (Nehme et al., 2020). Many of these sediments are surface derived, entering the caves via stream sinks or dissolution pipes (Laignel et al., 2004; Chédeville et al., 2015).

The Caumont cave system comprises a branchwork passage network intersected by underground quarrying, leaving truncated segments of cave passages (Rodet and Lautridou, 2003). The main segment of cave conduit is 2.4 km long, typically comprising a partially sediment-filled phreatic/epiphreatic passage (Ballesteros et al., 2020; Nehme et al., 2020) that drops from 20 to 8 m elevation towards the NE (Fig. 2). In the middle section, the main cave conduit splits into two branches, which re-join before diverging again into passages near the current explored limit to the NE (Fig. 2). The draining of the conduit by quarrying and excavation by speleologists has revealed many extraordinary sediment sections along the now largely relict conduit, sixteen of which were selected for detailed sedimentological and stratigraphical analysis (A-P on Fig. 2).

3. Methodology

3.1. Stratigraphical analysis

Allostratigraphy was applied to the detrital infill of the Caumont cave system since it considers bounding surfaces with time-stratigraphical significance such as erosion surfaces and speleothem horizons in order to compartmentalise discrete sediment packages (North American Commission on Stratigraphic Nomenclature, 1983). Sixteen allostratigraphical sections were logged in the northern half of the main cave conduit (Fig. 2a) to identify cave facies (Bosch and White, 2004; White, 2007) and depositional units. No sections were studied in the southern cave system because a permanent stream occupies the small conduit in this area rendering access difficult. The legend for the stratigraphical sections is shown in Fig. 3.

3.2. Gamma-ray spectrometry

In order to support the correlation between the stratigraphical sections, Gamma-ray spectrometry was applied in situ on fine-grained sediments. This technique is widely used in well logs for interpretation and correlation of Quaternary sedimentary facies (e.g., Nobre et al., 2020) as well as for characterising the radiative contribution of sediments for luminescence and ESR dating (e.g., Richard et al., 2021). Natural gamma-ray energy is related to the occurrence of clay minerals as major components, which are rich in ^{40}K and other radioactive isotopes belonging to the U series disintegration chain (Reinhardt and Herrmann, 2018). Sediments were measured by the application of the Digidart Gamma spectrometer (Ortec©) to 68 sampling points within sediments layers thicker than 15 cm (diameter of the gamma spectrometer). The gamma values depend primarily on the targeted horizon, and secondly on the surroundings including adjacent cave deposits and bedrock that can influence the measurement in a conic area of c. 20 cm. We assume that the bedrock contribution, which yielded extremely low gamma values, would be similar in all the sections, as the Caumont cave system is located in the same horizontal, laterally uniform Chalk beds (Ballesteros et al., 2022a). Gamma-ray activity is expressed in counts per seconds (cps) as a semi-quantitative result obtained from the average of 10 in situ-measurements.

3.3. Optical microscopy

An optical microscopy study was completed on thin sections to identify detrital microfacies and to detail their mineralogy, texture, sedimentary structures and provenance. Ten undisturbed sediment blocks were strategically carried out from eight stratigraphical sections using a Kubiena aluminium cubic box (1 L). Each box was rammed into the sediment using a hammer and covered by a plastic film for preserving wet conditions. Preparation of the thin sections was performed following Guilloré (1980) at the De la Préhistoire à l'Actuel: Culture, Environnement et Anthropologie (PACEA) laboratory (Université de Bordeaux, Centre Nationale de la Recherche Scientifique and Ministère de la Culture, France).

3.4. X-ray diffraction

X-ray diffraction (XRD) was conducted to identify: i) the main mineral groups forming the deposits, ii) the source area of detrital deposits, and iII) the palaeoenvironment of the cave surroundings during cave detrital sedimentation. Ten samples were collected from clayey-loamy layers detailed in six of the sections. Clay identification was conducted at XRD Analytical & Consulting CC, Lynnwood Glen (South Africa). Dried samples were milled, split, and powder prepared for XRD analysis using a back-loading preparation method (Brindley and Brown, 1988). Diffractograms resulted from a Malvern Panalytical Aeris diffractometer with PIXcel detector and fixed slits with Fe filtered Co-Kα radiation, whilst clay groups were identified using X'Pert Highscore plus software. Semi-quantitative estimations (weight %) were calculated using the Rietveld method. The detection limit is 0.5 % and amorphous phases were not considered. XRD was also applied to all samples after exposing to ethylene glycol during 3 days and heating to 550 °C for 3 h. New diffractograms do not exhibit any peak shift after ethylene glycol dissolution (except to sample ROB.B-11), indicating the occurrence of a non-

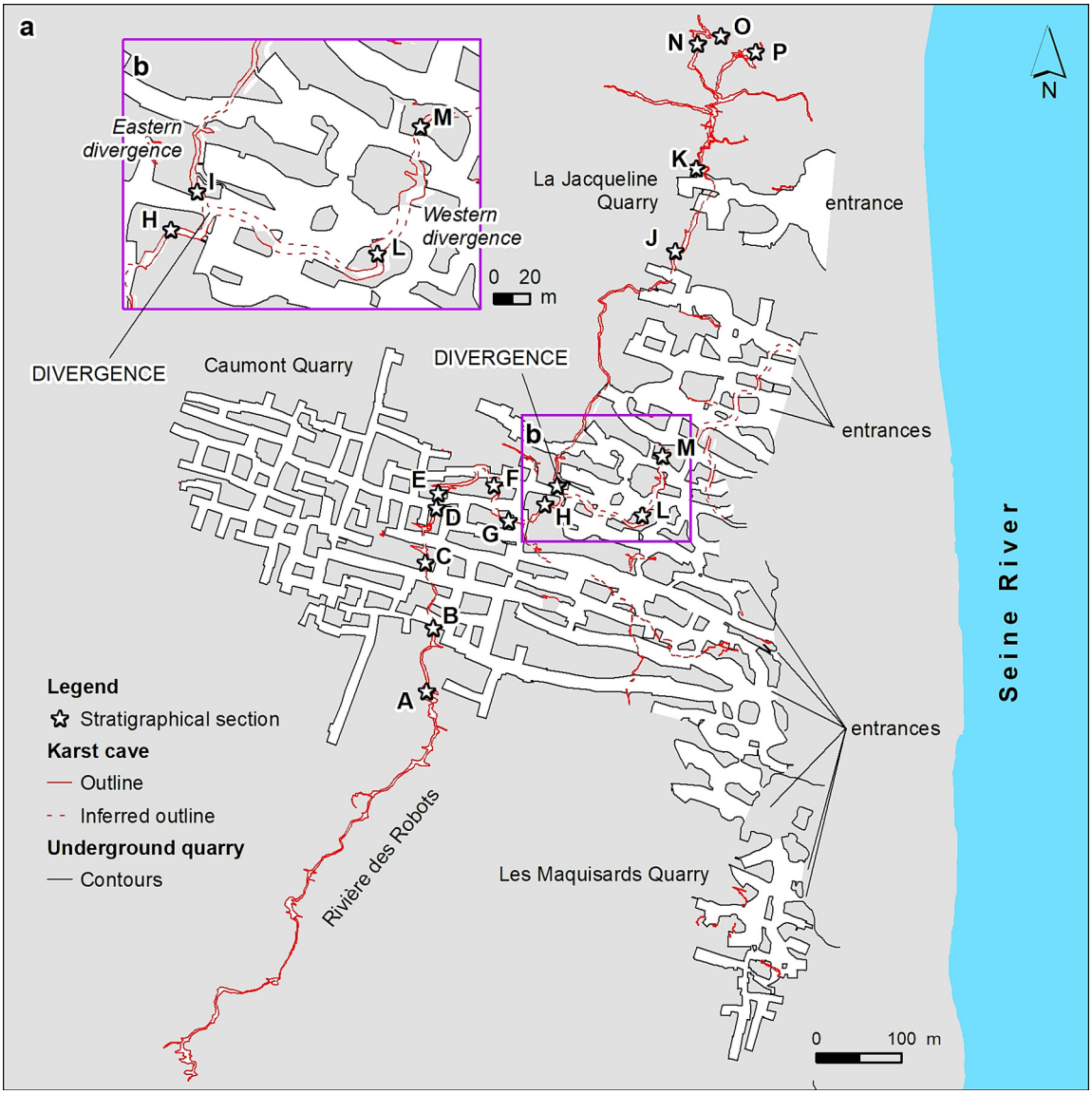

Fig. 2. (a) Location of the sixteen stratigraphical sections carried out along the Caumont cave system. (b) Inset showing detail around the conduit divergence. Cave and quarry map is after Ballesteros et al. (2022a).

swelling mineral. This mineral is likely to be vermiculite, not chlorite since the 7°A peak collapsed after heating. Only sample ROB.B-11 shown a peak shift after glycolation revealing the presence of smectite.

3.5. Geochronology

Speleothem U-series dating was used to constrain the cave deposition model. The nine speleothems selected for dating have compact and elongate calcite crystals under a microscope, sometimes with minor local overgrowths, and without any diagenetic textures (micritised crystals, corrosion crystal contacts, etc.), indicating the geochemical systems remained closed after precipitation. The $^{234}U/^{230}Th$ dating was performed at the NERC Isotope Geosciences Laboratory (British Geological Survey), Keyworth (United Kingdom). Powdered 100 to 400 mg samples were collected with a diamond-drill from each sample. Chemical separation and purification of U and Th were performed according to Edwards et al. (1987). Isotope concentrations were obtained on a Thermo Neptune Plus multi-collector inductively coupled plasma mass spectrometer (MC-ICP-MS) following procedures modified from Hellstrom (2006) and Heiss et al. (2012). Mass bias and scanning electron microscope gain for Th measurements were corrected using an in-house ^{229}Th-^{230}Th-^{232}Th reference solution calibrated against CRM 112a, whilst activity ratios were calculated considering the decay constants of Cheng et al. (2013). Quoted uncertainties for activity ratios, initial $^{234}U = {}^{238}U$ equilibrium and ages include a c. 0.2 % uncertainty calculated from the combined $^{236}U = {}^{229}Th$ tracer calibration uncertainty and measurement reproducibility of reference materials as well as the measured isotope ratio uncertainty. Ages were calculated from time of analysis (2021) in years before 1950 with two sigma uncertainty error (2σ). The effect of detrital contamination was corrected by calculating activity ratios and dates using a detrital isotope composition of $^{232}Th/^{238}U = 1.2$, $^{230}Th/^{238}U = 1.0$ and $^{234}U/^{238}U = 1.0$, with ±50 % (2σ) uncertainties.

The geochronological framework of cave sediment deposition was approached by a Bayesian hierarchical modelling based on Event modelling (Lanos and Philippe, 2018) with ChronoModel 2.0 software (Lanos and Dufresne, 2019). Such an approach was used to propose a holistic integrated chronology, combining individual dates (t_i), associated uncertainties and stratigraphical data into events (θ). The model was built utilising seven $^{234}U/^{230}Th$ ages obtained by Nehme et al. (2020) and new U-series dates acquired for this study. A Metropolis-Hastings algorithm (Robert et al., 2011) was applied assuming a Gaussian prior distribution for each date (Lanos and Philippe, 2018).

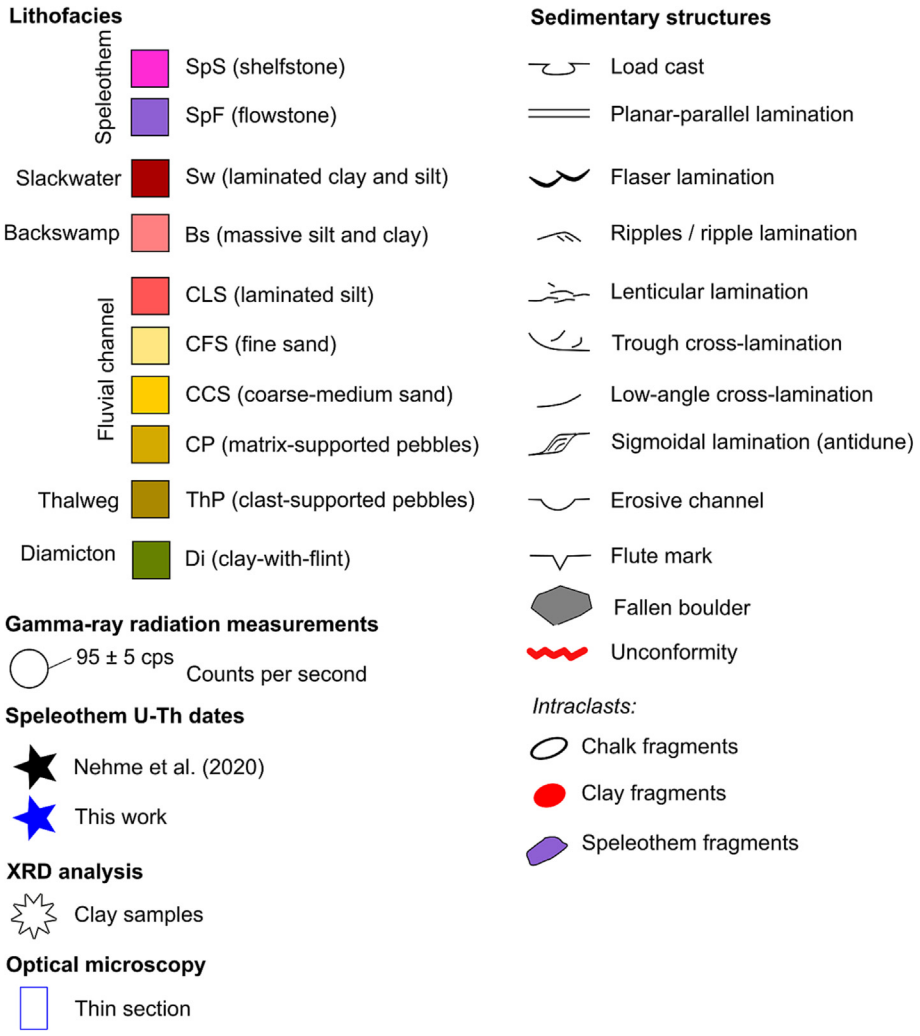

Fig. 3. Legend for the stratigraphical sections, identifying detailed cave facies, sedimentary structures, measurement of gamma-ray radiation and chronological data.

4. Results

4.1. Stratigraphical units

Figs. 4 to 7 show the stratigraphical logs along Caumont cave system (Fig. 2). The stratigraphy, facies and gamma-ray spectrometry data allowed us to define five allostratigraphical units bounded (summarised in Table 1) by erosive discontinuities. The thickness of the allostratigraphical units varies up to 3 m along the cave, showing significant lateral variability (Figs. 4-7). Moreover, depositional features in the western divergence conduit (Fig. 5) are different than the ones preserved in the eastern divergence conduit (Fig. 6). Locally, some units have been partially or completely eroded, resulting in an overall complex geometry shown mainly in both Units 2 and 3.

1) Allostratigraphical Unit 1 is formed by fining-upward sequences composed of orange-brown coarse sand (CCS facies) at the base, fining up to laminated silt (CLS facies) at the top (Figs. 4-6). In general, granulometry and sedimentary structures (planar-parallel lamination) of Unit 1 are mainly related to sediment-laden flows although the basal part of the succession shows massive beds associated with hyper-concentrated flows.
2) Allostratigraphical Unit 2 exhibits fining-upward sequences comprised of yellowish sub-angular gravel with a sandy matrix (ThP; CP facies) with an erosive base, a sandy bed (CCS; CFS facies) in the middle part and laminated silt (CLS facies) at the top (Figs. 4-6). The sandy bed shows planar-parallel, ripple, cross-lamination and sigmoidal lamination that reflect hydraulic conditions related to sediment laden flows whereas the angular pebbly sandy gravel resulted from hyper-concentrated flows with suspension load. The fining-upward sequences are interbedded by poorly sorted diamictic deposits made of flint cobbles and pebbles with a clayey loam matrix (Figs. 4-6). These are interpreted as debris flows that briefly disturbed the fluvial succession. Allostratigraphical Unit 2 is preserved on top of Unit 1 (Fig. 4 - sections A, E, F; Fig. 6 - section L) and comprises two perched flowstones (Fig. 4 - sections C, H).
3) Allostratigraphical Unit 3 comprises fining-upward sequences formed by yellowish-brown coarse to fine sand (CCS; CFS facies) (Figs. 4-6). The sequences include re-worked speleothem fragments and sedimentary structures (planar-parallel, ripple and cross-laminations) indicative of sediment laden flows. Unit 3 is stratigraphically above Unit 2 (Fig. 4 - sections C, F; Fig. 6 - section I) and the perched flowstone depicted in Fig. 6 - Section L is related to Unit 3.
4) Allostratigraphical Unit 4 was only recognised in the northern part of the Caumont cave system (Fig. 7- sections O, P). It consists of fining-upward sequences composed of yellowish-brown coarse-medium sand (CCS facies) in the lower half, passing up to fine sand (CFS facies) and laminated silt (CLS) at the top (Fig. 7). This unit includes also fallen speleothem fragments without any evidence of fluvial transport.
5) Allostratigraphical Unit 5 is represented by fining-upward sequences formed by beige-dark brown massive silt (Sw facies) at the base, massive clay-silt (Bs facies) in the middle-upper part of

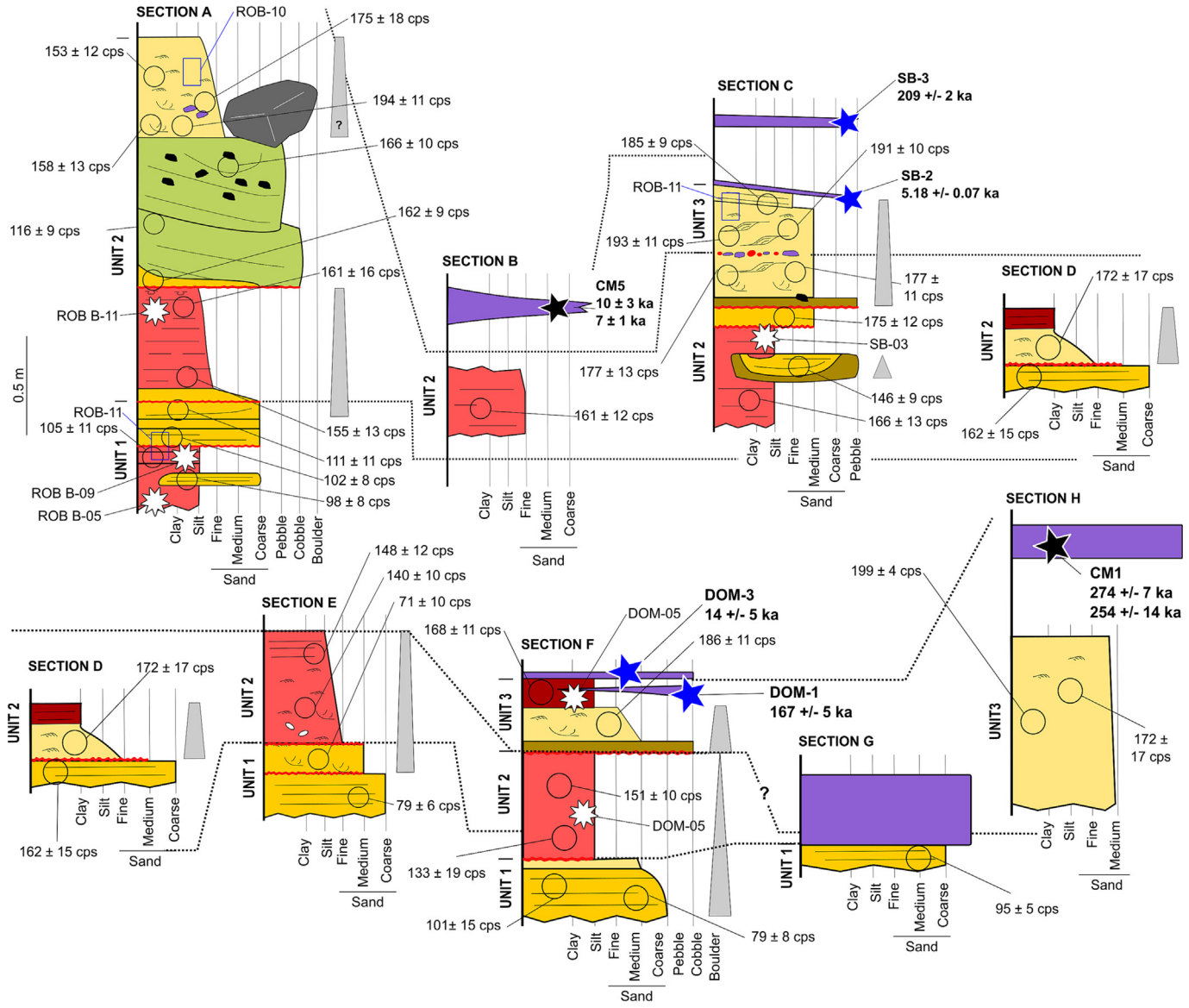

Fig. 4. Allostratigraphical units identified in sections A to G along the main conduit of Caumont cave system, from the SW to the divergence (Fig. 2). Section D is repeated to display stratigraphical correlation. Legend is shown in Fig. 3.

the sequence, and shelfstone and flowstone (Sp facies) precipitated on the top (Fig. 5). Unit 5 overlies Unit 2 in Section J (Fig. 4) and over Unit 3 in Section F (Fig. 4), where the contact between Units 3 and 5 is gradual and diffuse. Such facies associations probably result from the erosion and reworking of previous cave deposits.

4.2. Cave facies

Six facies were identified in the Caumont cave system combining field evidence (Fig. 8) and microscopical observations (Fig. 9). The ideal sedimentary sequence has 1–5 m thickness and starts with the deposition of thalweg facies followed by the sedimentation of channel, slackwater and backswamp facies, and ends with speleothem precipitation. The diamicton facies is coeval to the channel facies, resulting in debris flow deposits interbedded within the fluvial sediments.

a) The thalweg facies (thalweg pebbles, ThP) comprises clast-supported sediments dominated by pebbly gravel, followed by a fining-upward sequence of finer gravel and sand, within allostratigraphical Units 2 and 3 (Fig. 8a). The clasts are mainly flint, pedogenic fragments and rarely speleothem and Eocene limestone clasts, showing a weak clast imbrication. Pedogenic and limestone particles exhibit well to moderate rounding. The matrix contains fragments of flint, as well as metamorphic and igneous quartz. The base of the thalweg facies is typically an erosive surface, above which is fluvial sediments with paleochannel features in Sections C and M (Figs. 4-6; 8a). The facies represent bedload pebbles and sand deposited by cave streams after partial erosion of former Units 2 or 3.

b) The fluvial channel facies comprise coarse-medium sand (channel coarse sediment facies, CCS), fine sand (channel fine sediment, CFS) and laminated silt (channel lime-sand, CLS) seen in allostratigraphical Units 1 to 4 (Fig. 8a-b). In general, these layers show fining-upward graded beds with moderately to well-sorted sub-rounded to rounded grains of chert, metamorphic and igneous quartz and very little clay (Fig. 9a-b). Chalk sand to silt-size particles, speleothems clasts and pedogenetic particles are also present, especially in allostratigraphical Units 2–4. The CCS facies exhibits frequently planar-parallel and cross laminations under microscopy, whilst CFS and CLS facies show planar-parallel and ripple laminations (Figs. 8c; 9c-d). Channel facies were deposited on thalweg facies and derived from suspended and bedload silt-sand.

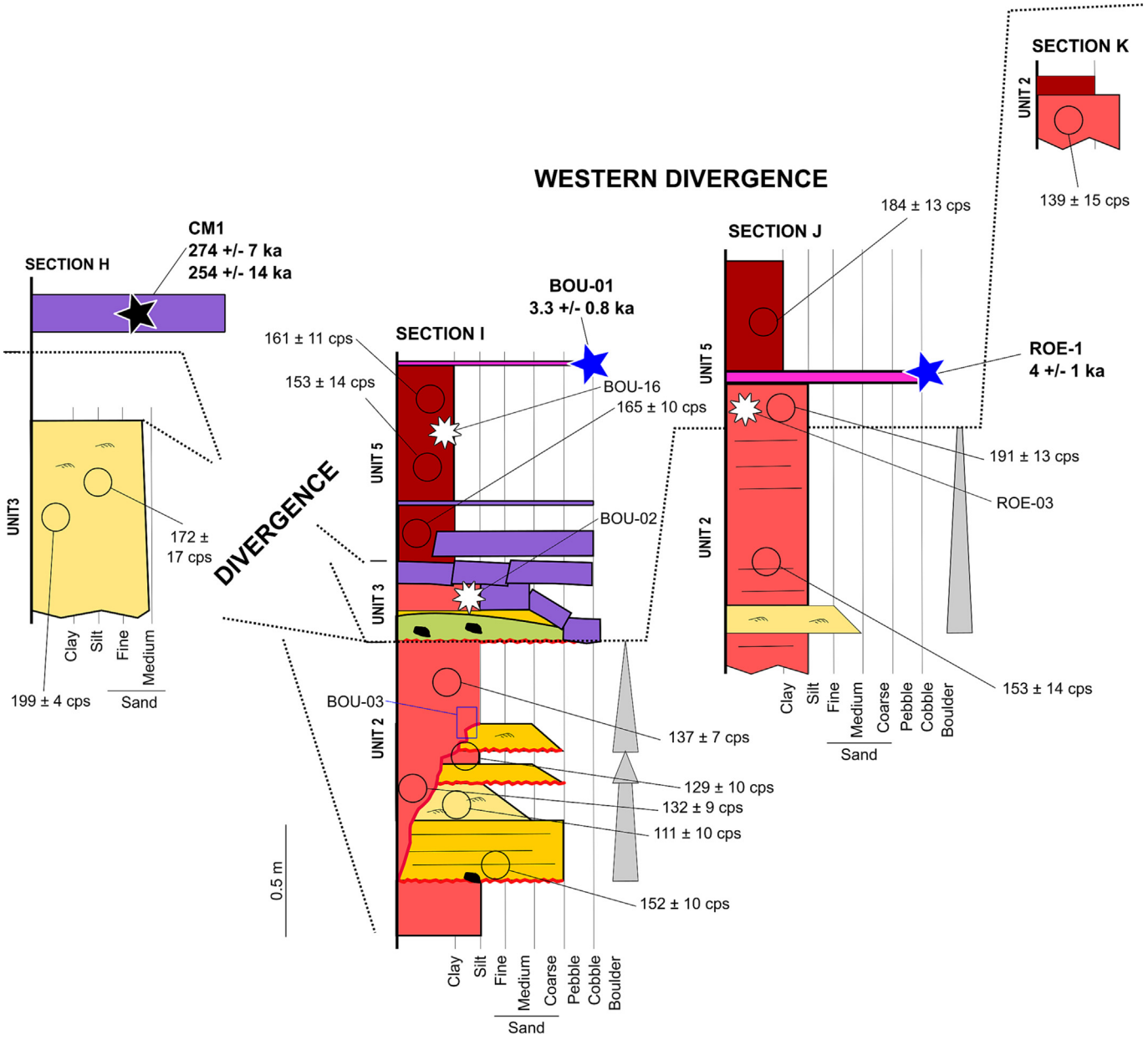

Fig. 5. Allostratigraphical units identified in sections H to K in the western divergence passages of the main conduit of Caumont cave system (Fig. 2). The figure displays the correlation between field observations and the bottom of section I. Legend is shown in Fig. 3.

c) The slackwater (Sw) facies is formed by laminated and poorly sorted silty and clayey beds, which dominates allostratigraphical Unit 5, and to a lesser extent, Unit 3. Sw facies exhibits fining-upward sequences made of angular to sub-angular silt composed of flint and other quartz and clay minerals (Fig. 9e-f) resulting from bed-load traction and subsequent decantation after a cave flood.

d) The backswamp (Bs) facies includes massive clay and minor silt (Fig. 8c), locally containing isolated flint and chalk angular clasts, as well as pedogenic fragments. In general, the sorting is poor. Bs facies were identified in allostratigraphical Unit 5 and locally, in Unit 2. The massive aspect of this facies suggests the rapid deposition of suspended fine-grained sediments, coeval with spalling of fragments from the local flinty chalk bedrock.

e) The speleothem facies comprise shelfstone (speleothem shelfstone, SpS) and flowstone (speleothem flowstone, SpF) precipitated in relation to allostratigraphical Units 2, 3 and 5. Both speleothems are dominated by columnar and elongated columnar fabrics following Frisia et al. (2000). SpS resulted from carbonate precipitation on a pool surface, occurring on slackwater facies, whilst SpF is formed on backswamp, slackwater and fluvial channel facies.

f) The diamicton (Di) facies corresponds to sub-angular flint and/or chalk clasts with a clayey-sandy matrix, showing a clast-supported or matrix-supported texture (Fig. 8d). Di facies is interbedded between fluvial channel facies of allostratigraphical Units 2 and 3, and resulted from a debris flow. These probably result from the mobilisation of the surface Clay-with-Flints deposits by debris processes and other mechanisms through sub-vertical shafts into the karstic conduits at depth.

4.3. Stratigraphical correlation

Gamma-ray measurements (displayed in Figs. 4 to 7) combined with stratigraphical and microscopical evidence helped identify five allostratigraphical units (Sections 4.1 and 4.2). In general, gamma-ray activity decreases from the bottom to the top of each stratigraphical section

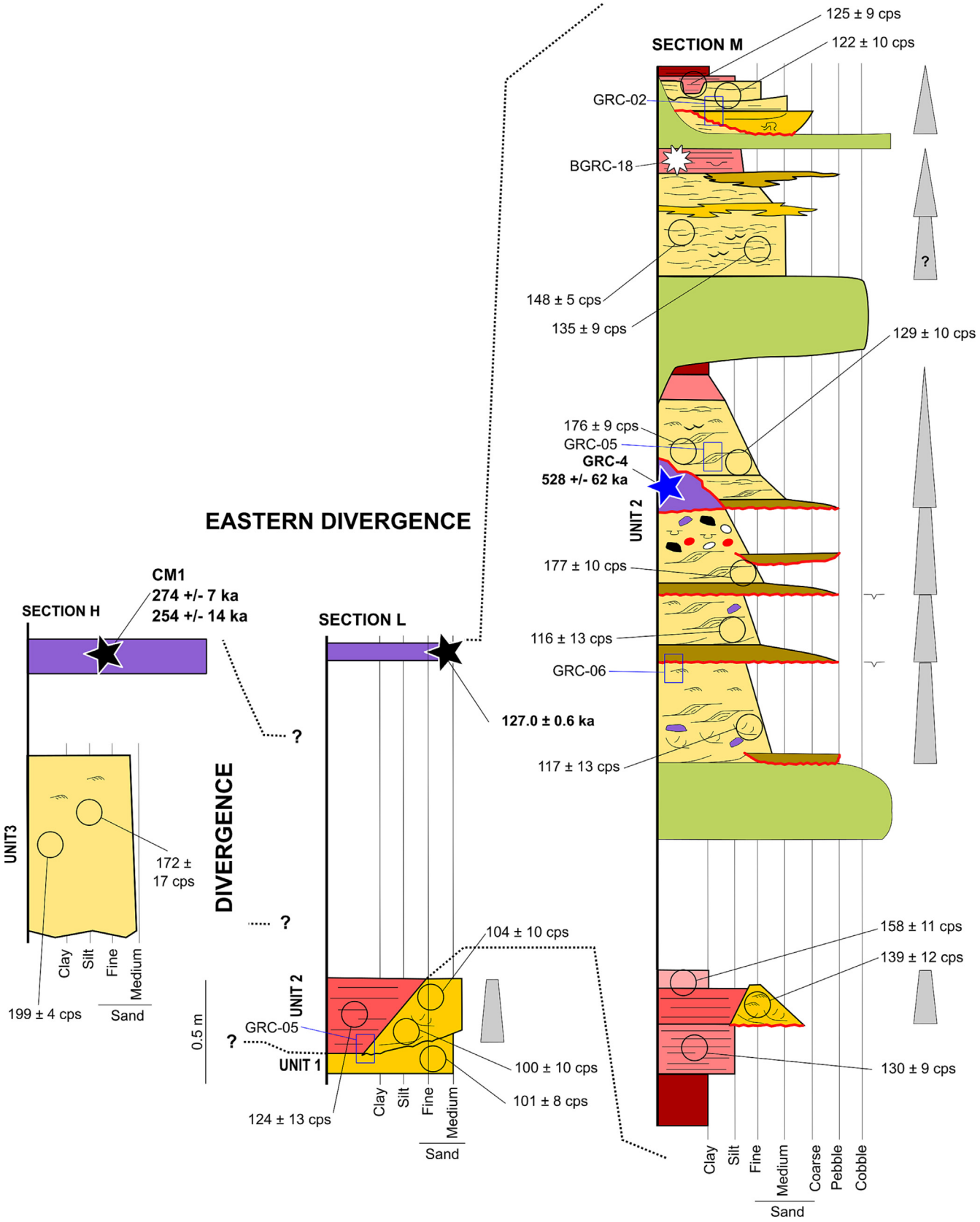

Fig. 6. Allostratigraphical units identified in sections H, L and M in the eastern divergence passages of the main conduit of Caumont cave system (Fig. 2). The picture displays the correlation between field observations and the top of section M. Legend is shown in Fig. 3.

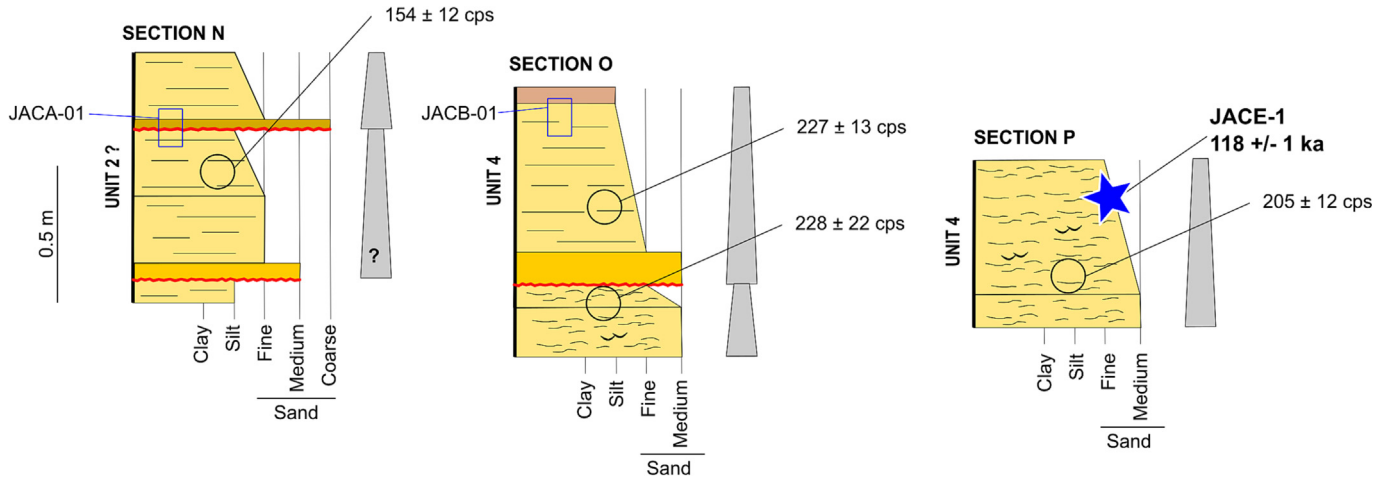

Fig. 7. Allostratigraphical units identified in sections N to P M in the northernmost part of the Caumont cave system (Fig. 2). Legend is shown in Fig. 3.

(Fig. 10), irrespective of the granulometry (Fig. S1 – Supplementary Data). Anomalous values were interpreted as the contribution of local factors; for example, the presence of a nearby speleothem fragments may have increased the gamma-ray contribution as sampled speleothems yield moderate to high uranium concentrations (Table 3). The gamma activity of Unit 3 (177–193 cps) overlaps the radiation values of Unit 5 (177–193 cps), which is close to the range of gamma-ray levels of Unit 2 (116–177 cps) (Fig. 10).

4.4. Mineralogy

More than 70 % of the fluvial channel and thalweg facies are composed of sub-angular flint (chert and other sedimentary quartz), 10–20 % sub-rounded metamorphic quartz (polycrystalline grains formed by sub-crystals with medium to strong undulose extinction, deformation lamellae and bands), 1–5 % opaque minerals (titanite, rutile, hematite and other Fe—Ti oxides and hydroxides), and 2–3 % carbonate fragments: calcite crystals and local chalk (Fig. 11). Plagioclase, K-feldspars, sub-rounded igneous quartz (monocrystal grains with mineral inclusions around crystal core), pedogenic grains (Fig. 11a, e), chalk fragments (Fig. 11f) and limestone rounded pebbles represent <1 % of studied deposits. Pedogenic fragments correspond to clay-quartz aggregates with an iron-mineral crusting (Fig. 12e-f), whilst limestone pebbles show non-coccolith bioclastic wacke- to grainstone textures.

Loamy layers are mainly formed by quartz (84–97 % of the sample), followed by clay minerals (2–11 %) and feldspars (1–7 %) (Table 2). Clay

Table 1
Main characteristics of the allostratigraphic units identified in Caumont cave system.

Allostratigraphic units	Facies association	Description	Lithofacies	Flow conditions	Gamma-ray activity (counts per second)	Chronological data
5	Slackwater	Fining-upward sequences of laminated silt to flowstone	Speleothem (Sp) Slackwater (Sw) Backswamp (Bsm)	Laminar or drip flow Calm water after flooding	139–199	• Local deposition finished in stratigraphic section I at 3.3 ± 0.8 ka (age of a flowstone located at the top of Unit 2) • Local deposition finished in stratigraphic section B at 7 ± 1 ka and 10 ± 3 ka (age of a perched flowstone) • Local deposition finished in stratigraphic section F at 14 ± 5 ka (age of a flowstone located on Unit 2)
4	Stream channel	Fining-upward laminated sequences of medium-fine sand to silt, including reworked speleothems	Fluvial sand and silt (CP, CCS, CFS, CLS)	Sediment laden flow	205–227	• Local deposition in stratigraphic section P after 118 ± 1 ka (age of a reworked speleothem fragment)
3	Stream channel	Fining-upward sequences of coarse-fine sand to silt, including reworked speleothems	Fluvial sand (CCS, CFS)	Sediment laden flow	177–193	• Local deposition in stratigraphic section L finished at 127.0 ± 0.6 ka (age of a perched flowstone) • Coeval to 167 ± 5 ka (age of an interbedded speleothem precipitated in situ) in stratigraphic section F
2	Stream channel with debris flow	Fining-upward sequences of pebbles to silt with interbedded diamictic deposits and reworked speleothems	Backswamp (Bsm) laminated silt (CLS) Fluvial sand and pebbles (CCS, CFS, CP) Thalweg (ThP)	Hyperconcentrated to sediment laden flow and occasional cohesive debris flow	116–177	• Local deposition in stratigraphic section C finished at 209 ± 2 ka (age of a perched flowstone) • Coeval to 528 ± 62 ka (age of an interbedded speleothem precipitated in situ) in stratigraphic section L
1	Stream channel	Fining-upward sequences of coarse sand to silt	Fluvial sand (CCS, CFS, CLS)	Hyperconcentrated to sediment laden flow	71–111	• No data

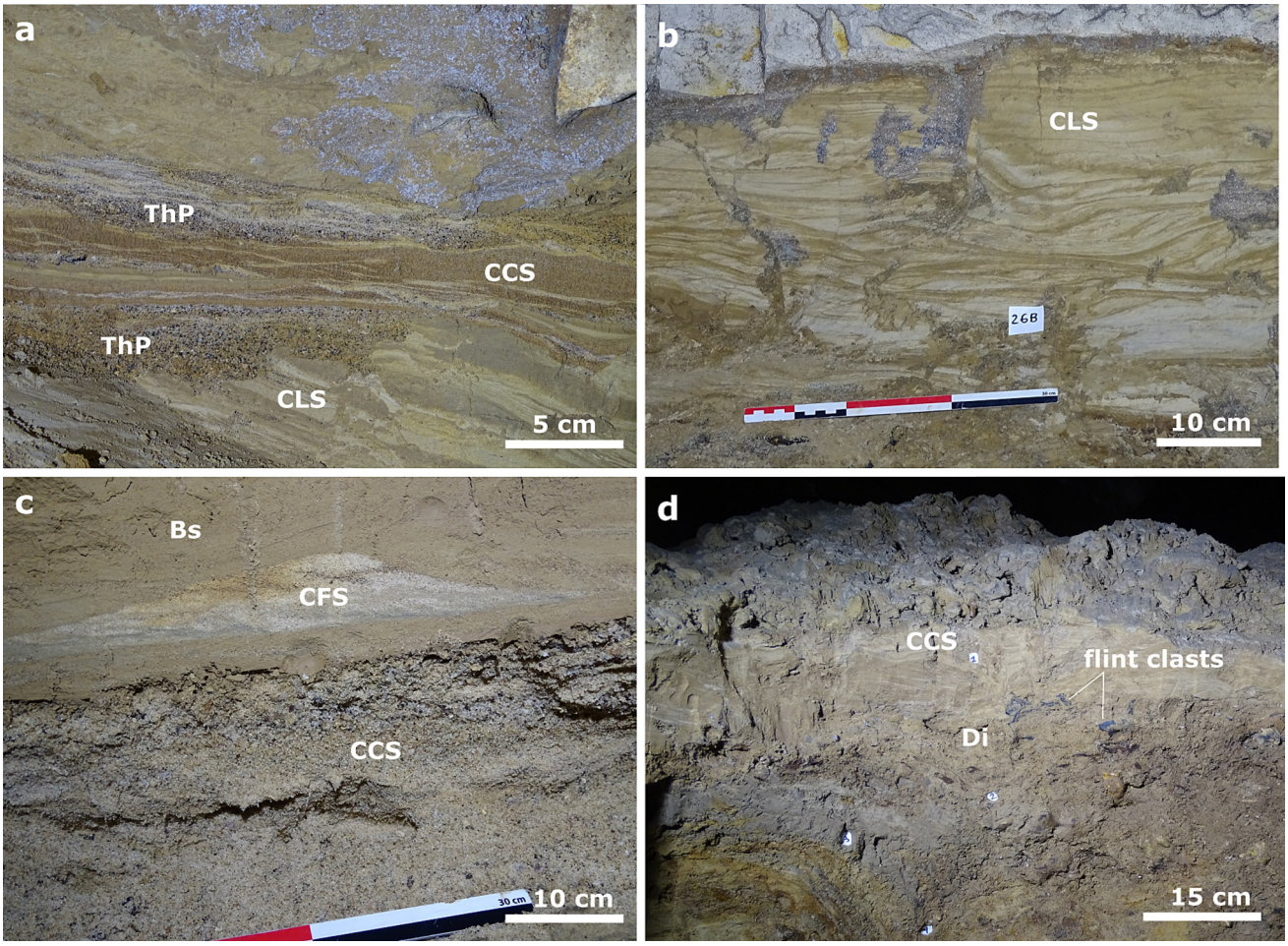

Fig. 8. Cave facies recognised in Caumont cave system: (a) middle part of section M (Fig. 6) showing thalweg facies (Thp), coarse-medium sand (CCS) and laminated silt (CLS). (b) Bottom of section O (Fig. 7) formed mainly by fine sand (CFS). (c) Section E (Fig. 4) displaying fine sand (CFS) forming a ripple within backswamp facies (Bs), deposited on coarse-medium sand (CCS). (d) Top of section A (Fig. 4) dominated by a diamicton facies (Di) made of Clay-with-Flint rich sediments.

minerals belong to: i) the kaolinite group (<7 %), not identified though in allostratigraphical Units 1 and 3, ii) the mica group (muscovite and/or illite) (<4 %), and iii) the vermiculite group (1–2 %). Smectite minerals (5 %) was only identified in one sample whilst feldspars comprise plagioclase (1–4 %) and K-feldspars as orthoclase (<3 %).

4.5. $^{234}U/^{230}Th$ dating

The nine $^{234}U/^{230}Th$ speleothem dates (Table 3) obtained from the Caumont cave system range from 3.3 ± 0.8 ka to 528 ± 62 ka providing chronological constraints to the allostratigraphical units. Detrital contamination is generally considered negligible if the $^{230}Th/^{232}Th$ ratio is greater than two. Therefore, the sample BOU-02 ($^{230}Th/^{232}Th$ ratio = 1.6) was discarded, leaving eight $^{234}U/^{230}Th$ ages for the chronological framework.

5. Discussion

5.1. Sources of cave detrital sediments

The bimodal size distribution of the sediments and their major and minor minerals suggest three possible sources for the detrital deposits in the Caumont cave system.

1) The main source of detrital material are the autochthonous flint nodules within the Chalk bedrock, both eroded from within the cave system and allogenic flints derived from the surface deposits. These deposits correspond to Clay-with-Flints and/or slope/periglacial deposits derived from them (Laignel et al., 1998, 2003). Another potential source is the flint-rich alluvial terrace deposits of the River Seine (Antoine et al., 2007).
2) A second significant source of allochthonous sediment is evident from the occurrence of typical metamorphic and igneous minerals within the cave infill, such as K-Ca-Na feldspars and metamorphic quartz. The likely source areas for these sediments would be: i) the Morvan massif located at the headwaters of the current River Seine, or ii) the French Massif Central, located 500 km SE of the Caumont cave system (Fig. 1). Even though located far from the direct catchment area of the cave, the Massif Central was part of the Seine-Loire catchment area during the Pliocene and early Quaternary (Tourenq and Pomerol, 1995; Westaway, 2004). Both sources imply the contribution of the River Seine to the detrital sedimentation within the Chalk aquifer. This probably occurred when the river recharged the aquifer following a rise in the base-level, as occurs in the Seine basin at the present day (Flipo et al., 2020), or by fluvial under-capture across meander necks.
3) The third source is the soil, superficial deposits and Eocene limestone that cover the Chalk plateau (Van Lint et al., 2003). Limestone pebbles and soil fragments can be transported by runoff, suffosion and infiltration processes from the karst plateau into the Caumont cave system. The roundness of the Eocene limestone pebbles implies some fluvial transport before transportation into the endokarst, suggesting the occurrence of small streams on the Normandy plateau in the past.

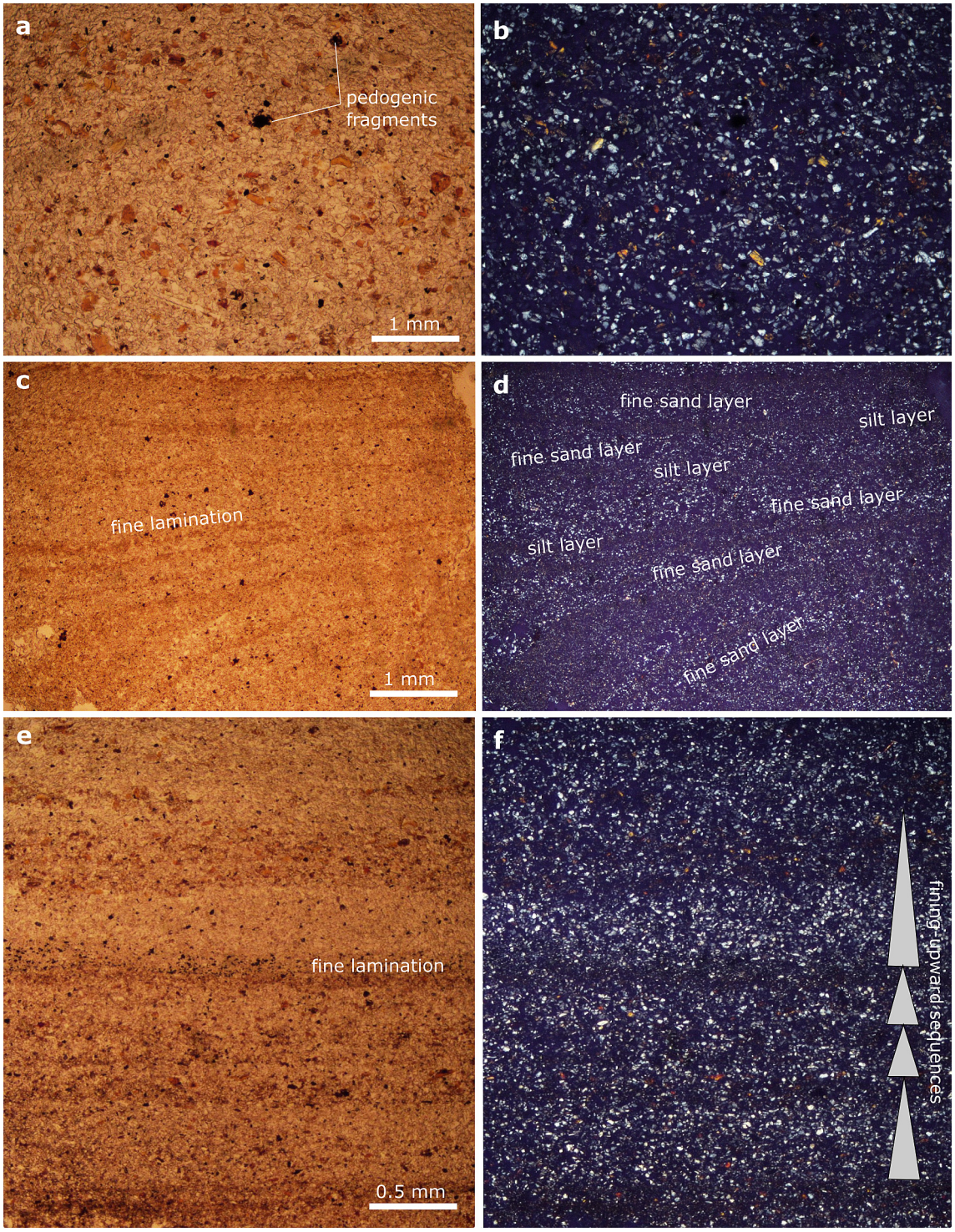

Fig. 9. (a) Massive coarse-medium sand showing pedogenetic fragments (under natural light). (b) Same view than an under polarised light. (c) Fine lamination by the alternation of fine sand and silt (under natural light), associated with bedload silt-sand. (d) Same view than c under polarised light. (e) Fine lamination formed by fining-upward graded silt. (f) Same view than e under polarised light.

The first source is common in those Chalk caves studied in Normandy, for example the Petites Dales, Villequier II and Orival-Foulon caves (Laignel et al., 2004; Rodet et al., 2006; Chédeville et al., 2015). Nevertheless, the main source of the sediment in these caves is the aeolian sediment that was deposited on the Chalk plateau during the last glacial period (Lautridou et al., 1999). Loess-derived-sediment was not recognised within the Caumont cave system, at least, not in allostratigraphical units 1–3. On the contrary, the metamorphic and igneous minerals, soil fragments and Eocene limestone clasts identified in the Caumont cave system have not been identified in any other Normandy Chalk caves.

5.2. Palaeoenvironmental conditions from clay mineralogy

The clay mineral populations found within the Caumont cave system infill are significantly different to those found in the Chalk (Laignel et al., 2004) and surface deposits of Normandy plateau, which comprise loess deposits, the fluvial-marine St-Eustache Sand Formation (Lautridou

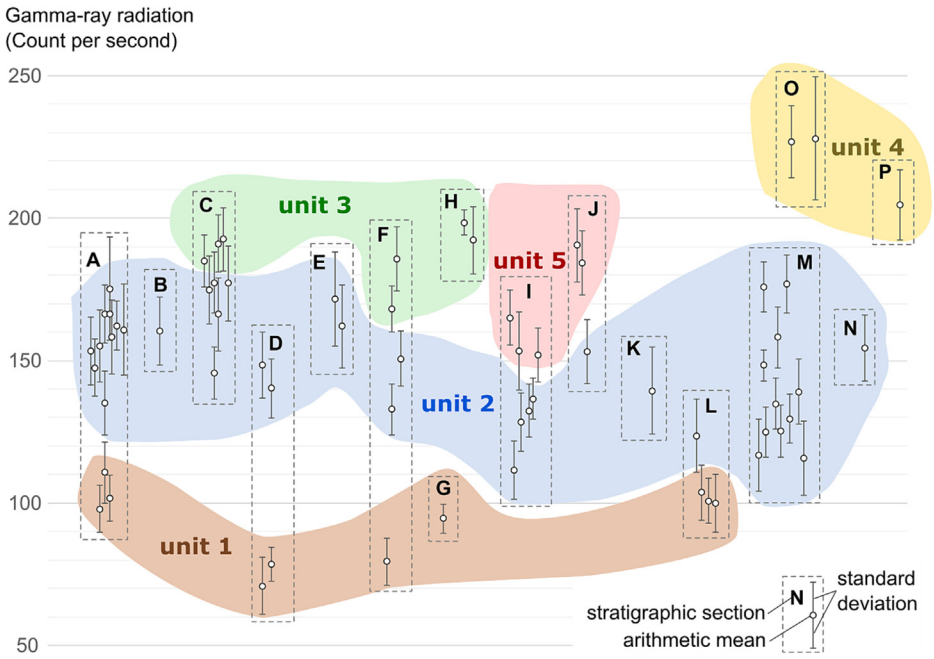

Fig. 10. Gamma-ray radiation measured in studied sections (A to P) and its correspondence to the allostratigraphical units (Table 1) defined in Caumont cave system.

et al., 1999), and Clay-with-Flints deposits (Laignel et al., 2002). In the Petites Dales and other chalk caves, detrital sediments derived from the loess have a distinctive smectite-kaolinite-illite signature (Laignel et al., 2004; Rodet et al., 2006), which is absent at Caumont. All of this suggests that clay minerals reported in the present study are not related to the local bedrock or are derived from the surface deposits, nor are they significantly affected by pedogenetic process (Fig. 12). Kaolinite is commonly formed by the chemical weathering of feldspar, mica, pyroxene, or amphibole under relatively warm and wet conditions, whilst the origin of illite is mainly related to the physical erosion of rocks under cold and dry conditions (Chaudhri and Singh, 2012). However, the interpretations rely on three assumptions. (1) We assume that clay formed at the plateau surface has been quickly introduced into Caumont cave system, thus clays identified in allostratigraphical units are related to palaeoenvironmental conditions occurring on the Normandy plateau at the time. (2) Clay differentiation during transport due to particle size or differential flocculation (Singer, 1984) may overlap clay abundance reported in cave sediments. (3) Diagenetic clay occurs within the Chalk sequence of the Paris basin, often as thin marl beds (Deconinck et al., 2005). The abundance of diagenetic illite in the cave sediments is three to six times higher than the kaolinite content preserved within the Coniacian Chalk.

Allostratigraphical Unit 1 includes mica (e.g. illite, others) but not kaolinite (Fig. 12). This clay assemblage most probably formed on the karst plateau surface under cold/dry conditions, possibly during glacial periods. On the contrary, allostratigraphical Units 2–5 show similar abundance of kaolinite and mica, which suggests a regional relatively temperate/humid climate.

5.3. Chronology

The oldest dated sample (GRC-04) at 528 ± 62 ka (Fig. 6 - section M) corresponds to a flowstone interbedded within allostratigraphical Unit 2 (Fig. 14a), although it shows a large uncertainty. Therefore, the deposition of Unit 1 might have occurred prior to 528 ± 62 ka and the formation of Unit 2 is coeval to ~528 ± 62 ka. Speleothem CM2 is a flowstone precipitated in dissolution pockets dated to 301 ± 20 ka (Nehme et al., 2020). Such dissolution pockets are widely spread along the main conduit but not associated with any visible allostratigraphical unit. Speleothem CM1 dated at 274 ± 7 and 250 ± 14 ka (Nehme et al., 2020) is a perched flowstone deposited on sediments. The sediments were subsequently eroded by water flows (Fig. 4 - section H).

The age of the perched flowstone SB-3 (209 ± 2 ka) reported in section C (Fig. 4) is older than the speleothem SB-2 (5.18 ± 0.07 ka), located stratigraphically below (Fig. 14b). This configuration reveals an apparent chronological reversal: in fact, SB-3 was precipitated on sediments deposited prior to the Holocene and was partially removed after ~5 ka. The detrital deposit would correspond then to Units 2 or 3 according to section C. Unit 3 has an interlayered flowstone DOM-01 (Fig. 4 - section F) dated at 167 ± 5 ka (MIS 6), when Unit 3 was being deposited. Therefore, SB-3 was probably precipitated prior or during the deposition of Unit 2.

The perched flowstone (CM3) was also formed on a previously eroded deposit (Figs. 6 - section L; 14C). Its age at 127.0 ± 0.6 ka (Nehme et al., 2020) is consistent with the position and timing of Unit 3, hence CM3 should precipitate above this unit. JACE-1 consists of speleothem fragments within Unit 4 and was dated at 118 ± 2 ka in section P (Fig. 7). Therefore, the deposition of Unit 5 took place after the precipitation of JACE-01.

Flowstone DOM-3 (Fig. 4 - section F) was dated at 14 ± 5 ka and is preserved on top of Unit 5. Thus, DOM-3 marks the ending of the local detrital deposition of Unit 5. The last perched flowstone (CM5) is reported in section B (Fig. 4) and was dated at 10 ± 3 and 7 ± 1 ka (Nehme et al., 2020). According to these dates, the CM5 precipitated on top of Unit 5, which was artificially removed by quarrymen. Similarly, flowstone ROE-1 precipitated at 4 ± 1 ka, on top of Unit 5 (Fig. 5 - section J), revealing that this unit was coeval with the early Holocene period.

5.4. Age of the cave

Based on speleothem and palaeomagnetic dating, Nehme et al. (2020) suggested a model for cave development and incision in the Seine valley. This coupled with the dates acquired for this study indicates that the lower level conduits in the Caumont system were formed earlier than 528 ± 62 ka, but after the Brunhes-Matuyama reversal (781 ka). Once the cave system developed, continued base-level lowering drained the conduit by at least 528 ± 62 ka, causing vadose incision, the development of vadose shafts, and deposition of speleothem. The conduit was partially filled by a complex

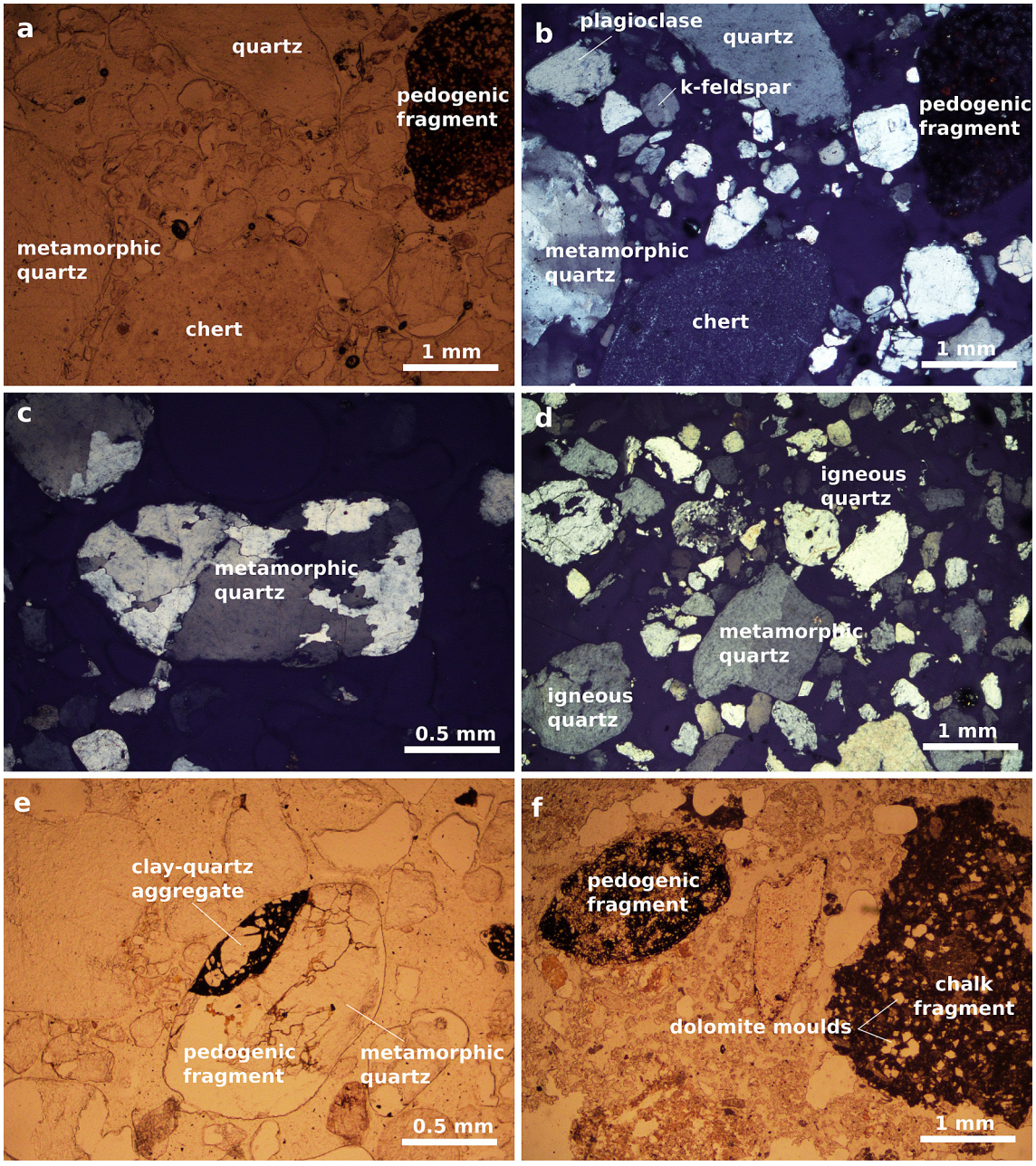

Fig. 11. Coarse-medium sand facies (CCS): (a) Sub-rounded grains of chert and other sedimentary quartz, metamorphic quartz (showing undulose extinction) and pedogenetic fragment (natural light). (b) Same view than an under polarised light. (c) Rounded grain of metamorphic quartz formed by sub-crystals with irregular and deformed limits. (d) Sub-rounded grains of igneous quartz and other types under polarised light. (e) Rounded pedogenic fragment composed by a clay-quartz aggregate and a quartz metamorphic grain. (f) Pedogenic fragment and dedolomitised chalk fragment, which is similar than the chalk bedrock of the Caumont cave system reported by Ballesteros et al. (2022b).

succession of fluvial sediments, breakdown deposits and speleothems dated from ~301 to ~7 ka (Nehme et al., 2020).

5.5. Depositional model of the Caumont Chalk cave system

The inferred age of the allostratigraphical units was plotted on the first chronological model carried out for a Chalk cave (Fig. 13). The model is more realistic since MIS 7 and comprises five depositional phases (Table 4; Fig. 15) after the formation of the phreatic conduit and its subsequent paragenetic evolution and vadose entrenchment (Nehme et al., 2020). After deposition, Units 1–4 were partially eroded resulting in a paraconformity between Units 1 and 2 and a clear erosion surface between the remaining Units.

Detrital deposition began with allostratigraphical Unit 1 (Fig. 15a) sometime after the Brunhes-Matuyama reversal (781 ka) and continued until 528 ± 62 ka (Fig. 13). Unit 2 was deposited around 528 ± 62 ka until 209 ± 2 ka (MIS 7), marked by the precipitation of a large flowstone SB-3 (Fig. 15b). The third phase began between ~209 and ~167 ka and finished at ~127 ka with the precipitation of speleothem CM-3 on fluvial sandy deposits (Fig. 13d). The conduit was completely filled at this date as at previous times. The deposition of allostratigraphical Unit 4 occurred after ~118 ka (the age of speleothem JACE-1) and finished sometime during the Late Pleistocene (Fig. 15f). The final phase corresponds to the deposition of allostratigraphical Unit 5 within the eastern divergence conduit during the Late Pleistocene and finished at 10–7 ka (Fig. 15h). Finally, speleothem growth occurred at the top of the allostratigraphical Units 2–3 and 5 during interglacials (Fig.13), notably MIS 7, 5e (Eemian) and 1 (early Holocene).

Sediment aggradation during phases 1–3 (or previous non-identified times) and consequent upwards dissolution led to the

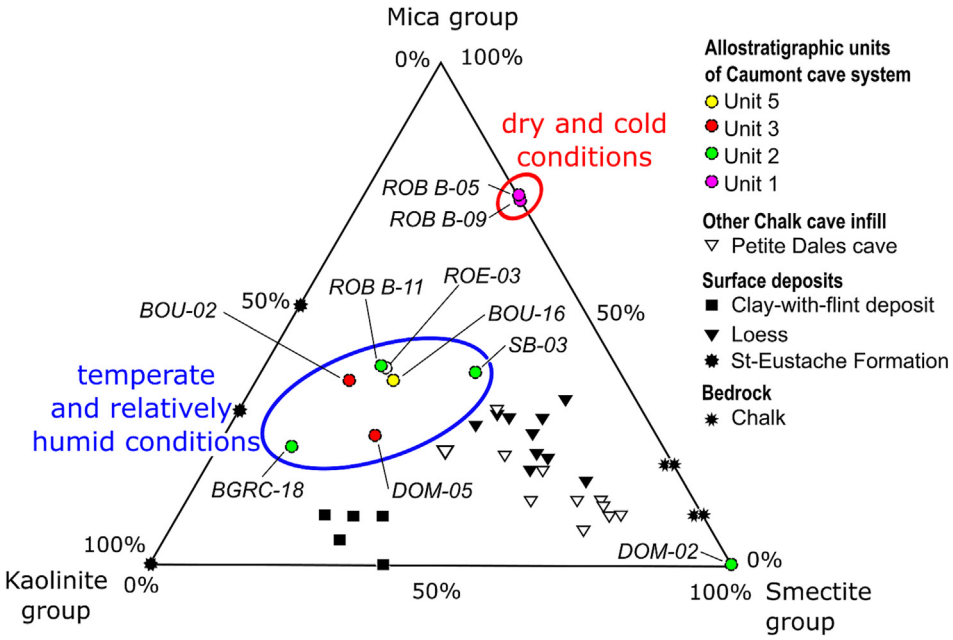

Fig. 12. Clay relative content of loamy layers from Caumont cave system, suggesting regional environmental conditions developed during the formation of clay minerals on the Normandy plateau. Minerology of the Chalk and surface deposits is from Laignel et al. (2002, 2004), whilst the clay contain of the Petite Dales cave infill from Rodet et al. (2006).

development of paragenetic passage morphologies identified in Caumont cave system (Farrant and Smart, 2011; Nehme et al., 2020; Ballesteros et al., 2020). The divergence of the Caumont main conduit probably occurred during Phase 3. Units 2–3 may obstruct the western conduit leading to its abandonment and the subsequent development of the eastern conduit, with younger detrital sediments and significantly younger speleothems. Phase 3 and, probably, the previous one, were coeval with a major sedimentary aggradation in many karst caves along the European Atlantic margin during the MIS 7–6 (Proctor et al., 2005; Lundberg and McFarlane, 2007; Aranburu et al., 2015; Arriolabengoa et al., 2015, 2018, 2020; Ballesteros et al., 2017, 2019; Harmand et al., 2017). The deposition coincided with the end of the Penultima (Saalian) Glacial Cycle (Graham et al., 2011) and would be related to a major period of denudation reported in the English Channel in MIS 6 (Mellett et al., 2013), as well as the formation of fluvial terraces in Seine valley between 206 and 162 ka (MIS 7) (Durbet et al., 1997). Earth eccentricity shows a maximum during MIS 7–6 favouring the development of warmer summer and colder winters in the North Hemisphere (Berger and Loutre, 1991). This climatic contrast combined with periglacial processes may increase denudation rates producing abundant sediments at the surface (Murton and Belshaw, 2011).

Units 1, 2 and 3 resulted from hyper-concentrated and sediment-laden flows that deposited coarse to fine-grained sediments within a fluvial channel (Fig. 15). These sediments show a relative-abundance of igneous and metamorphic quartz that were transported by the River Seine from the Morvan and/or French Central Massif (Section 5.1) and washed into the cave system. Furthermore, the first depositional phase includes abundant mica that originated probably under a dry and cold regional climate (Section 5.2). The occurrence of pedogenic grains within Units 2–4 would indicate a significant development of soils on the karst plateau from the mid-Chibanian to the Late Pleistocene. These soils had clay minerals that would be formed under relatively temperate and humid conditions.

The deposition of Units 2–3 was periodically interrupted by cohesive debris flows that bought additional surface material derived from the surface Clay-with-Flints deposits via solution pipes to the cave stream channel (Fig. 15b). This process is very common in the Chalk across Europe (Quesnel et al., 2003; Stenestad, 2006; Dobrowolski et al., 2012). Debris deposits were not reported in Units 1 and 4–5 deposited in the Caumont cave system, suggesting the main formation of solution pipes was coeval to Units 2–3, deposited from 528 ± 62 to 127.0 ± 0.6 ka. The dissolution pipes were probably entirely filled by surface sediments generated during MIS 7–6.

Sediment-laden flows also produced the stream channel facies that filled nearly all of the cave passages in the northern part of the Caumont cave system (Fig. 15f). Clay and silt decantation occurred within still

Table 2
Semi-quantitative (%) XRD analysis of 10 loamy layers from Caumont cave system.

Sample	Allostratigraphic units	Quartz	Feldspar		Clay				Total
			Orthoclase	Plagioclase	Mica group	Kaolinite group	Vermiculite group	Smectite group	
BGRC-18	2	84	2.4	2.2	2.6	7.0	1.4		99.6
BOU-02	5	86	2.7	4.1	2.8	3.6	1.2		100.4
BOU-16	2	95		1.6	1.1	1.2	0.7		99.6
DOM-02	3	97		1.6			0.5		99.1
DOM-05	2	89	1.7	3.3	1.5	2.8	1.5		99.8
ROB B-05	1	96	1.1	1.1	1.3		0.5		100.0
ROB B-09	1	96	0.7	0.5	1.6		0.6		99.4
ROB B-11	2	87	1.3	1.6	2.2	2.2	1.1	4.6	100.0
ROE-03	2	86	1.7	1.1	4.3	4.4	2.2		99.7
SB-03	2	90	1.1	3.0	2.3	1.5	2.2		100.1

Table 3
Summary of new $^{234}U/^{230}Th$ data from Caumont cave system. Location section corresponds to the stratigraphic sections (Figs. 4-7). All uncertainties are reported at the 2σ level. Activity ratios calculated using the decay constants of Cheng et al. (2013). 1) Corrected activity ratios and dates calculated using a detrital $^{234}U/^{230}Th$ isotope composition of $^{232}Th/^{238}U = 1.2$, $^{230}Th/^{238}U = 1$ and $^{234}U/^{238}U = 1$ with ±50 % (2σ) uncertainties. 2) The uncertainty includes 0.2 % external reproducibility. 3) The uncertainty includes 0.1 % external reproducibility.

Sample Name	Location Section	^{238}U (ppm)	^{232}Th (ppm)	$^{230}Th/^{232}Th$ measured	$^{232}Th/^{238}U$ corrected	$^{234}U/^{238}U$ corrected	p_{08-48}	Uncorrected Age (ka)	Corrected Age (ka BP)	Initial $^{234}U/^{238}U$
DOM-03	F	0.4621	0.119	2.5	0.0846 ± 0.084	1.2695 ± 2.99	0.243	20.2 ± 0.1	13.9 ± 4.6	1.2804 ± 0.040
DOM-01	F	0.3125	0.091	9.9	0.0953 ± 0.149	1.1655 ± 2.40	0.904	174.0 ± 1.4	166.8 ± 5.4	1.2650 ± 0.046
SB-03	C	0.2402	0.001	777.3	0.0011 ± 0.139	1.0195 ± 0.14	0.027	208.8 ± 1.8	208.7 ± 1.8	1.0350 ± 0.002
SB-02	C	0.5509	0.002	51.0	0.0009 ± 0.149	0.9844 ± 0.15	0.093	5.3 ± 0.0	5.2 ± 0.1	0.9842 ± 0.002
GRC-04	M	0.0784	0.000	1024.5	0.0010 ± 0.137	1.0465 ± 0.31	0.001	528.5 ± 62.4	528.3 ± 62.4	1.2064 ± 0.026
BOU-01	I	0.5347	0.025	3.3	0.0152 ± 0.147	1.2336 ± 0.55	0.197	4.5 ± 0.0	3.3 ± 0.8	1.2358 ± 0.007
BOU-02	I	0.6067	0.103	1.6	0.0560 ± 0.145	1.2354 ± 2.02	0.207	8.5 ± 0.0	4.2 ± 3.1	1.2382 ± 0.026
ROE-01	J	0.5287	0.040	2.4	0.0248 ± 0.218	1.2415 ± 0.92	0.188	5.5 ± 0.0	3.5 ± 1.3	1.2439 ± 0.012
JACE-01	P	0.1423	0.007	45.2	0.0168 ± 0.149	1.1297 ± 0.49	0.708	119.0 ± 0.8	117.6 ± 1.2	1.1808 ± 0.008

waters after floods, coevally with the precipitation of shelfstone and flowstone at the top of Unit 5 (Fig. 15h). Such shelfstones occur in many cave passages (Fig. 5 – section I, J). The slackwater sediments may be associated with flooding caused by conduit sedimentary blockage and/or a rise in the water-table during the early Holocene sea-level maximum (Lambeck, 1997).

In conclusion, the detrital deposition within the Chalk resulted in a complex cave infill made of many depositional sequences since at least the Chibanian (Fig. 15), divided by erosional surfaces and sedimentary hiatuses.

5.6. Detrital sedimentation in Chalk caves

Fluvial and debris-flow sediments observed in the Caumont cave system are comparable to those seen in many classical karst caves (e.g., Campaña et al., 2017; Martini et al., 2018). This reinforces the idea, based on previous geomorphological and hydrogeological studies (see Farrant et al., 2023; Maurice et al., 2023), that the Chalk often acts as a karstic aquifer. In detail, the lithofacies and facies association established by Bosch and White (2004) and White (2007) for classical karst caves was successfully applied to the study of a Chalk aquifer conduit system for the first time. Fluvial sediments within conduits are characteristic of well-developed karst aquifers as they imply the presence of connected conduit network large enough to transport sediment through the aquifer (Goeppert and Goldscheider, 2019; Bettel et al., 2022). Likewise, a well-organised channelised underground conduit network (e.g., Piccini, 2011; Martini, 2011; Bella et al., 2021) is needed to generate the sedimentary structures observed. Most Chalk caves and conduit systems, both in the Caumont system, and in other Chalk caves in Normandy and elsewhere (Laignel et al., 2004; Rodet et al., 2006; Stenestad, 2006; Willems et al., 2007; Dobrowolski et al., 2012; Chédeville et al., 2015; Grube et al., 2017), are typically infilled with fine-grained sediments rather than the coarse allogenic sediments often seen in limestone caves (e.g., Häuselmann et al., 2010; Arriolabengoa et al., 2020). This reflects the small size of the allogenic catchments, the dominance of sand and clay-rich cover materials, notably loessic deposits and the Clay-with-Flint (Chédeville et al., 2015), the low hydraulic gradients in Chalk areas (Fournier et al., 2007, 2008; Sanz et al., 2016), and the typically small nature of the conduits limiting sediment transport in the Chalk aquifer. Chalk conduits typically have a much greater abundance of coarse autochthonous detrital sediment, mainly flint. Chalk clasts undergo rapid dissolution and disaggregation, so are typically quite rare.

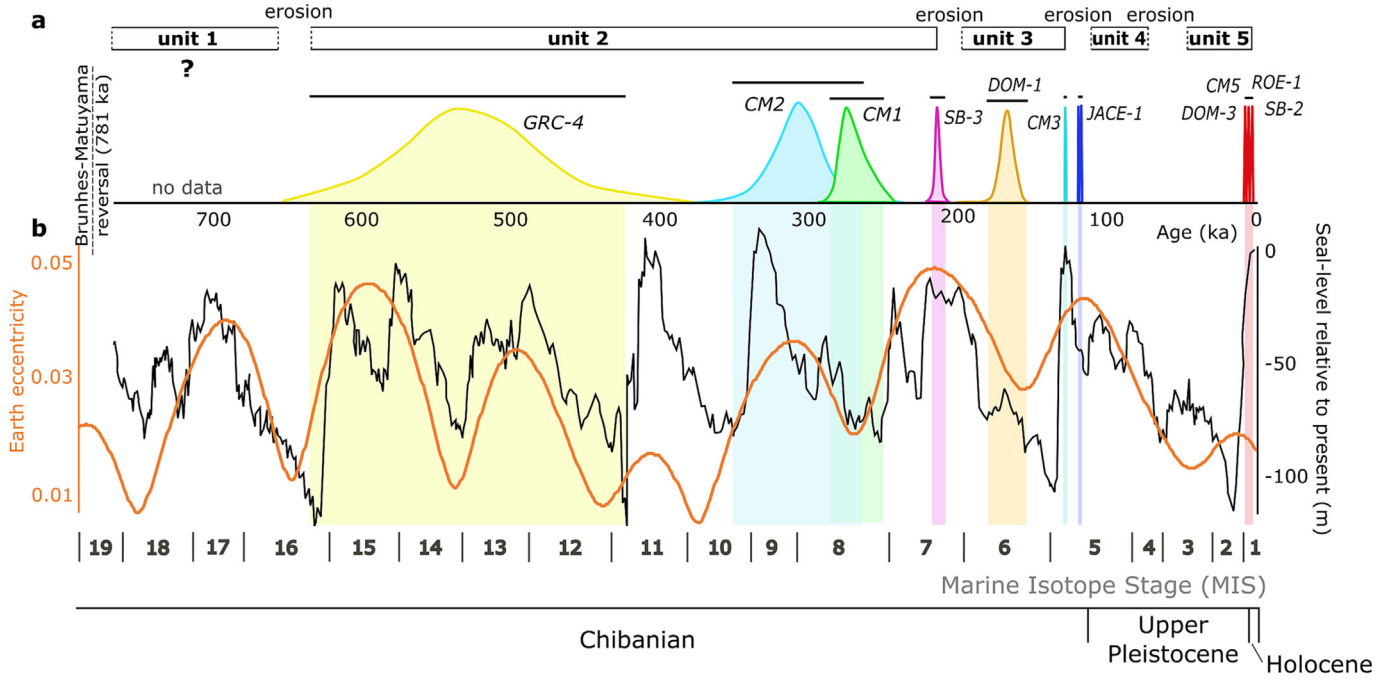

Fig. 13. (a) Chronology of the allostratigraphical Units 2 to 5 based on Bayesian modelling of 15 speleothem age density functions. Unit bars represent the constrained periods for potential unit sedimentation, which would not be continuous; confidence bars (95 %) are shown. (b) Earth eccentricity movement (Berger and Loutre, 1991) and global average relative sea-level oscillations (Rohling et al., 2021).

Table 4
Depositional phases defined in Caumont cave system from the Chibanian to Holocene.

Depositional phase	Allostratigraphic unit	Deposition process	Constrained age (ka)		Inferred palaeonvironment
			Start	End	
1	1	Hyperconcentrated flow Sediment-laden flow	<781	≥528 ± 62	Cold/dry conditions
2	2	Hyperconcentrated flow Sediment-laden flow Debris flow	≤528 ± 62	~209 ± 2	Relatively temperate/humid conditions
3	3	Sediment-laden flow	209 ≤ x ≤ 167	~127.7 ± 0.7	
4	4	Sediment-laden flow	<118 ± 1	?	
5	5	Calm water after flooding	?	~14–3	

5.7. Detrital sedimentation impact on Chalk aquifers

The Caumont cave system is representative of conduit systems in the Chalk aquifer that are entirely or partially infilled by sediments. Similar sediment filled conduits are exposed in coastal or quarry sections from United-Kingdom (Reeve, 2021) to Ukraine (Dobrowolski et al., 2012). To transport flint pebbles and sand as bedload, flow velocities of ca. 0.1–3 $m \cdot s^{-1}$ are required considering calculations based on Bosch and White (2004). These inferred velocities are estimations for vadose flows through Chalk conduits, and the highest values probably correspond to flood or storm events since they exceed velocities based on Chalk cave sediments (Laignel et al., 2004; Rodet et al., 2006; Chédeville et al., 2015) or sink to spring travel times based on tracer tests (Maurice et al., 2023).

The influx of significant amounts of fluvial sediment into a conduit alters the way it behaves and evolves over time. Sediment aggradation in the Caumont cave system and in other caves along the Seine valley (Nehme et al., 2020) armoured the conduit floor and favoured per ascension dissolution and subsequent paragenetic conduit development (Farrant and Smart, 2011). The influx of detrital sediment and periodic blockages leading to increased heads help facilitate the development of alternative flow paths, triggering conduit bifurcation (Section 5.5), creating an anastomotic mesh of conduit flow-pathways. This can cause flow divergence to multiple springs. Before modelling, field observations should be carried out to identify the extent and style of conduit development, for instance, from borehole wall images (e.g., Maurice et al., 2012), natural cliffs and escarpments (Lamont-Black and Mortimore, 2000) or open quarries (e.g., Grube et al., 2017).

6. Conclusions

The first depositional model was carried out for a Chalk cave optimising stratigraphical logs, microscopy, and speleothem $^{234}U/^{230}Th$ dating, as well as the novel application of gamma-ray spectrometry for correlating stratigraphical sections along the karst conduit. The proposed depositional model identifies five sedimentary units separated by periods of erosion that initiated prior to the mid-Chibanian. The units include

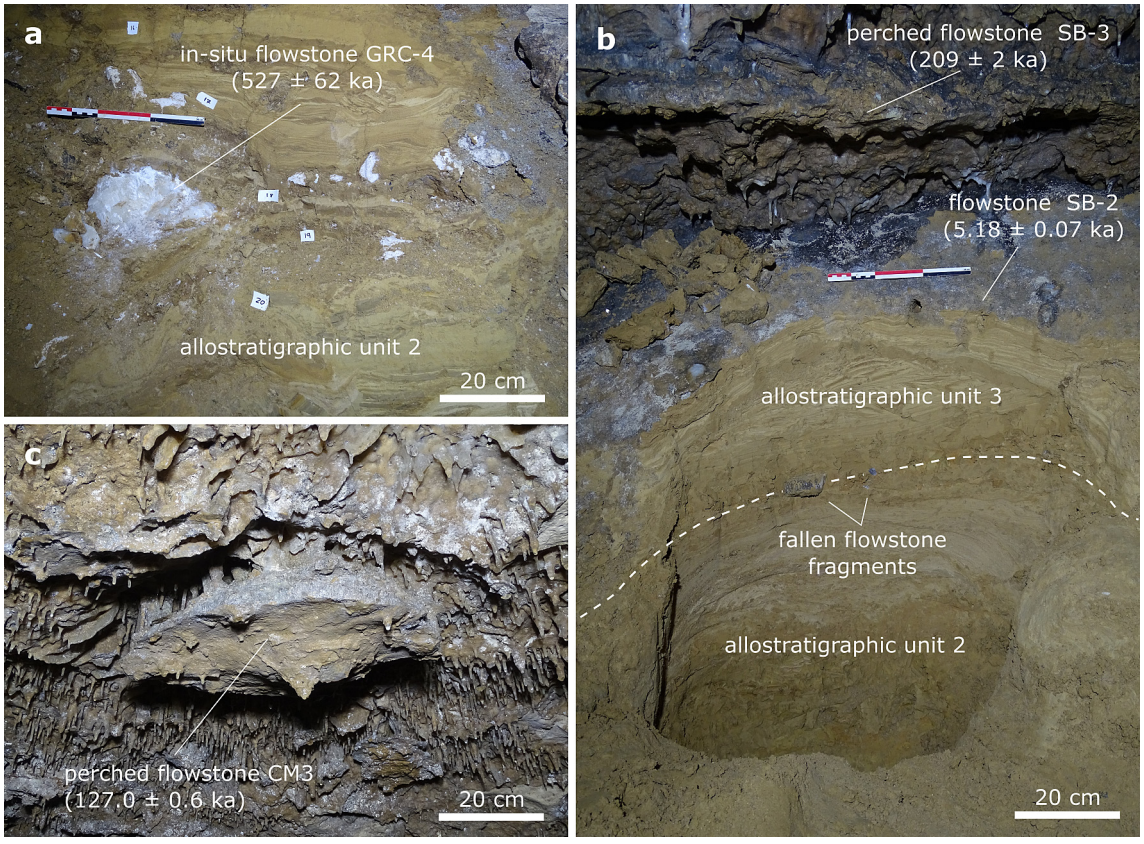

Fig. 14. Examples of speleothems dated by the $^{234}U/^{230}Th$ method to infer the chronology of allostratigraphical units: (a) in-situ flowstone GRC-4 interbedded within stratigraphical Unit 2. (b) Apparent inverted dates marked by flowstone SB-3, perched above Units 3 and 2, and by flowstone SB-2 precipitated on Unit 3; the limit between Units 2 and 3 is evidenced by the occurrence of fallen speleothem fragments related to the collapse of flowstone SB-3 after the partial erosion of underlying detrital units. (c) Flowstone CM3 precipitated on an already eroded fluvial deposit at ~127 ka (Nehme et al., 2020).

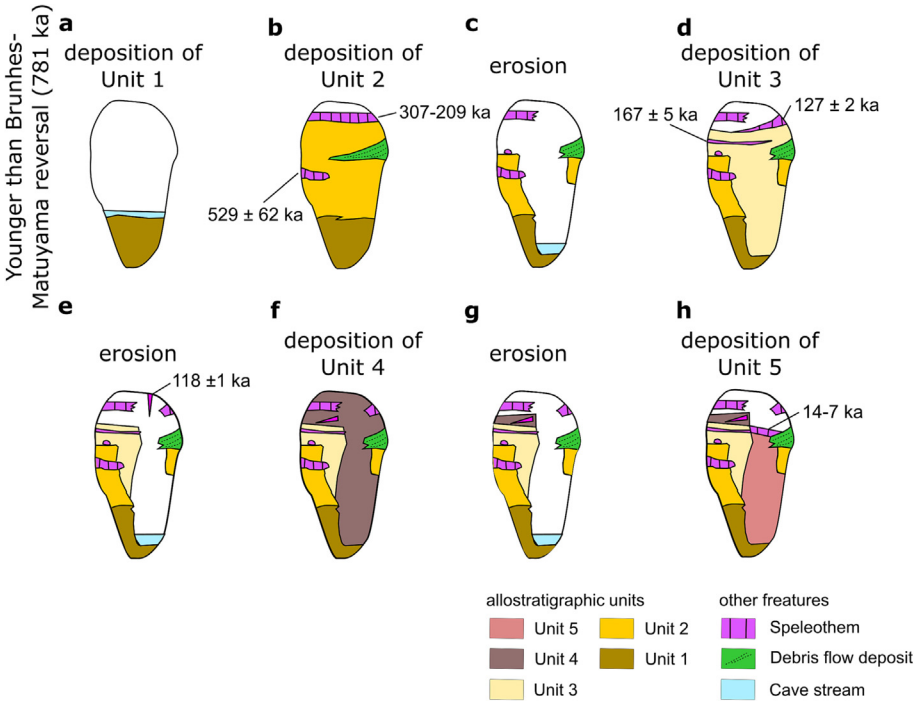

Fig. 15. Depositional model of Caumont cave system showing the sedimentation of the allostratigraphical units and the chronological data: (a) Deposition of allostratigraphical Unit 1 after 781; roof pendants and other paragenetic features reported in Nehme et al. (2020). (b) Deposition of allostratigraphical Unit 2 from before 529 ka to 209 ka. (c) Partial erosion of Units 1–2 between 209 and prior to 167 ka. (d) Deposition of allostratigraphical Unit 3 from earlier 167 ka to 127 ka. (e) Partial erosion of Units 1–3 between 127 and a time after 118 ka. (f) Deposition of allostratigraphical Unit 4 after 118 ka. (g) Partial erosion of units 1–4 long before 14 ka. (h) Deposition of allostratigraphical Unit 5 prior to 7 ka.

detrital sediment and speleothem precipitated mainly during climate optimum periods although exceptions occurred during MIS 6. The detrital sediment resulted from hyper-concentrated and sediment-laden flows that deposited coarse to fine-grained sediments within a fluvial channel. These vadose flow velocities were estimated to be ca. 0.1–3 $m \cdot s^{-1}$ during extraordinary floods and storms. The detrital sediment is composed mainly of authigenic flint from cave walls and allochthonous clay, flint and pedogenic aggregates derived from surface deposits via mainly solution pipes and vadose shafts active during mid to late Chibanian. The clastic sediment within the caves also contains metamorphic and igneous quartz and feldspar derived from the erosion of the Morvan massif and/or the Massif Central and transported by the Seine River into the Chalk aquifer.

The depositional model provides the sedimentological evidence to consider the Chalk as a karst media. In fact, detrital deposition shows a significant impact on the conduit development and groundwater flow in the Chalk aquifer. Sedimentary aggradation favours per ascension dissolution and enlargement of conduits (paragenesis), as well as conduit obstruction and the subsequent formation of new conduits by flow divergence. The occurrence of sediment-filled conduits can modify the dynamics and pathways of groundwater flow. Consequently, tracer tests and hydrological simulation should consider the potential occurrence of sediment-filled conduits in any Chalk area.

Supplementary data to this article can be found online at https://doi.org/10.1016/j.sedgeo.2023.106422.

Data availability

Data will be made available on request.

Declaration of competing interest

The authors declare that they have no known competing financial interests or personal relationships that could have appeared to influence the work reported in this paper.

Acknowledgments

This research was undertaken under the PALECONOR project funded by Région Normandie. We greatly indebted to Paul Rabelle and other speleologists belonging to Comité Régional de Spéléologie de Normandie for their valued support. We also thank Pierre Voinchet (UMR CNRS HNHP and Muséum National d'Histoire Naturelle, Paris) for providing facilities for Gamma-ray spectrometry. The mobile gamma spectrometer was purchased with the help of Ile-de-France regional council's Sesame and Labex BcDiv programmes. DB belongs to the Plan Andaluz de Investigación, Desarrollo e Innovación 2020 (Junta de Andalucía, Spain). ARF and DS publish with the approval of the Executive Director, British Geological Survey. Augusto Auler and other Reviewer are thanked for their careful and thoughtful reviews.

References

Antoine, P., Lautridou, J.P., Laurent, M., 2000. Long-term fluvial archives in NW France: response of the Seine and Somme rivers to tectonic movements, climatic variations and sea-level changes. Geomorphology 33, 183–207.

Antoine, P., Coutard, J.P., Gibbard, P., Hallegouet, B., Lautridou, J.P., Ozouf, J.C., 2003. The Pleistocene rivers of the English Channel region. Journal of Quaternary Science 18, 227–243.

Antoine, P., Limondin Lozouet, N., Chaussé, C., Lautridou, J.P., Pastre, J.F., Auguste, P., Bahain, J.J., Falguères, C., Galehb, B., 2007. Pleistocene fluvial terraces from northern France (Seine, Yonne, Somme): synthesis, and new results from interglacial deposits. Quaternary Science Reviews 26, 2701–2723.

Aranburu, A., Arriolabengoa, M., Iriarte, E., Giralt, S., Yusta, I., Martínez-Pillado, V., del Val, M., Moreno, J., Jiménez-Sánchez, M., 2015. Karst landscape evolution in the littoral area of the Bay of Biscay (North Iberian Peninsula). Quaternary International 364, 217–230.

Arriolabengoa, M., Iriarte, E., Aranburu, A., Yusta, I., Arrizabalaga, A., 2015. Provenance study of endokarst fine sediments through mineralogical and geochemical data (Lezetxiki II cave, northern Iberia). Quaternary International 364, 231–243.

Arriolabengoa, M., Iriarte, E., Aranburu, A., Yusta, I., Arnold, L.J., Demuro, M., Arrizabalaga, A., 2018. Reconstructing the sedimentary history of Lezetxiki II cave (Basque Country, northern Iberian Peninsula) using micromorphological analysis. Sedimentary Geology 372, 96–111.

Arriolabengoa, M., Intxaurbe, I., Ángeles, M., Alcaide, M., Rivero, O., Garaizar, J.R., Líbano, I., Aranburu, A., Cheng, H.A.I., Edwards, R.L., Garate, D., 2020. From cave geomorphology to Palaeolithic human behaviour: speleogenesis, palaeoenvironmental changes and

archaeological insight in the Atxurra-Armiña cave (northern Iberian Peninsula). Journal of Quaternary Science 35, 841–853.
Ballesteros, D., Rodríguez-Rodríguez, L., González-Lemos, S., Giralt, S., Álvarez-Lao, D.J., Adrados, L., Jiménez-Sánchez, M., 2017. New evidence of sea-level lowstands and paleoenvironment during MIS 6 and 4 in the Cantabrian coastal karst: the Cobiheru cave (North Iberia). Earth Surface Processes and Landforms 42, 1704–1716.
Ballesteros, D., Giralt, S., García-Sansegundo, J., Jiménez-Sánchez, M., 2019. Quaternary regional evolution based on karst cave geomorphology in Picos de Europa (Atlantic Margin of the Iberian Peninsula). Geomorphology 336, 133–151.
Ballesteros, D., Farrant, A., Nehme, C., Woods, M., Todisco, D., Mouralis, D., 2020. Stratigraphical influence on chalk cave development in upper Normandy, France: implications for chalk hydrogeology. International Journal of Speleology 49, 187–208.
Ballesteros, D., Nehme, C., Roussel, B., Delisle, F., Pons-Branchu, E., Mouralis, D., 2022a. Historical underground quarrying: a multidisciplinary research in the Caumont quarry (c. 13th–19th centuries), France. Archaeometry 64, 849–865.
Ballesteros, D., Painchault, A., Puente-Berdasco, B., Nehme, C., Todisco, D., García-Alonso, J.I., Varano, M., Mouralis, D., 2022b. Sourcing of chalkstone used in medieval buildings in the Eastern Duchy of Normandy (10th–14th centuries) through geological and geochemistry analyses. Geoarchaeology 37, 497–521.
Bella, P., Gradziński, M., Hercman, H., Leszczyński, S., Nemec, W., 2021. Sedimentary anatomy and hydrological record of relic fluvial deposits in a karst cave conduit. Sedimentology 68, 425–448.
Berger, A., Loutre, M.F., 1991. Insolation values for the climate of the last 10 million years. Quaternary Science Reviews 10, 297–317.
Bettel, L., Fox, J., Husic, A., Zhu, J., Al Aamery, N., Mahoney, T., Gold-McCoy, A., 2022. Sediment transport investigation in a karst aquifer hypothesizes controls on internal versus external sediment origin and saturation impact on hysteresis. Journal of Hydrology 613, 128391. https://doi.org/10.1016/j.jhydrol.2022.128391.
Bosch, R.F., White, W.B., 2004. Lithofacies and transport of clastic sediments in karstic aquifers. In: Sasowsky, I.D., Mylroie, J. (Eds.), Studies of Cave Sediments. Kluwer Academic/Plenum Publishers, New York, pp. 1–22.
Bouchaou, L., Mangin, A., Chauve, P., 2002. Turbidity mechanism of water from a karstic spring: example of the Ain Asserdoune spring (Morocco). Journal of Hydrology 265, 34–42.
Brindley, G.W., Brown, G., 1988. Crystal Structure of Clay Minerals and Their X-ray Identification. Mineralogical Society, London (518 pp.).
Campaña, I., Benito-Calvo, A., Pérez-González, A., Ortega, A.I., Bermúdez de Castro, J.M., Carbonell, E., 2017. Pleistocene sedimentary facies of the Gran Dolina archaeo-paleoanthropological site (Sierra de Atapuerca, Burgos, Spain). Quaternary International 433, 68–84.
Chaudhri, A.R., Singh, M., 2012. Clay minerals as climate change indicators—a case study. American Journal of Climate Change 1, 231–239.
Chédeville, S., Laignel, B., Rodet, J., Todisco, D., Fournier, M., Dupuis, E., Girot, G., Hanin, G., 2015. The sedimentary filling in the chalk karst of the Northwestern Paris Basin (Normandy, France): characterization, origin and hydro-sedimentary behaviour. Zeitschrift für Geomorphologie 59, 79–101.
Cheng, H., Edwards, L.R., Shen, C.C., Polyak, V.J., Asmerom, Y., Woodhead, J., Hellstrom, J., Wang, Y., Kong, X., Spötl, C., Wang, X., Alexander, E.C., 2013. Improvements in 230Th dating, 230Th and 234U half-life values, and U-Th isotopic measurements by multi-collector inductively coupled plasma mass spectrometry. Earth and Planetary Science Letters 371-372, 82–91.
Crampon, N., Roux, J.C., Bracq, P., 1993. France. In: Downing, R.A., Price, M., Jones, G.P. (Eds.), The Hydrogeology of the Chalk of North-West Europe. Clarendon, Oxford, pp. 113–152.
Culshaw, M.G., Waltham, A.C., 1987. Natural and artificial cavities as ground engineering hazards. Quarterly Journal of Engineering Geology & Hydrogeology 20, 139–150.
Deconinck, J.F., Amédro, F., Baudin, F., Godet, A., Pellenard, P., Robaszynski, F., Zimmerlin, I., 2005. Late Cretaceous palaeoenvironments expressed by the clay mineralogy of Cenomanian-Campanian chalks from the East of the Paris Basin. Cretaceous Research 26, 171–179.
Descamps, F., Faÿ-Gomord, O., Vandycke, S., Schroeder, C., Swennen, R., Tshibangu, J.P., 2017. Relationships between geomechanical properties and lithotypes in NW European chalks. Geological Society Special Publication 458, 227–244.
Dobrowolski, R., Fedorowicz, S., 2007. Glacial and periglacial transformation of palaeokarst in the Lublin-Volhynia Region (SE Poland, NW Ukraine) on the base of TL dating. Geochronometria 27, 41–46.
Dobrowolski, R., Mroczek, P., 2015. Clay cortex in epikarst forms as an indicator of age and morphogenesis—case studies from Lublin–Volhynia chalkland (East Poland, West Ukraine). Geomorphology 247, 66–75.
Dobrowolski, R., Bieganowski, A., Mroczek, P., Ryżak, M., 2012. Role of periglacial processes in Epikarst morphogenesis: a case study from Chełm Chalk Quarry, Lublin Upland, Eastern Poland. Permafrost and Periglacial Processes 23, 251–266.
Dugué, O., Lautridou, J.P., Quesnel, F., Clet, M., Poupinet, N., Bourdillon, C., 2009. Évolution sédimentaire cénozoïque (Paléocène à Pléistocène inférieur) de la Normandie. Quaternaire 20, 275–303.
Durbet, G., Rodriguez, P., Badalian, L., Hadjouis, D., Gauthier, A., Laurent, M., Ricard, J.L., Wattez, J., 1997. Découverte d'un site Paléolithique moyen dans des alluvions saaliennes du confluent Seine-Marne à Maisons-Alfort (Val-de-Marne). Comptes Rendus de l'Académie des Sciences 324, 505–512.
Edmonds, C.N., 2008. Karst and mining geohazards with particular reference to the Chalk outcrop, England. Quarterly Journal of Engineering Geology & Hydrogeology 41, 261–278.
Edwards, R., Chen, J., Wasserburg, G., 1987. U-238-U-234-Th-230-Th-232 systematics and the precise measurement of time over the past 500,000 years. Earth and Planetary Science Letters 81, 175–192.
El Janyani, S., Massei, N., Dupont, J.P., Fournier, M., Dörfliger, N., 2012. Hydrological responses of the chalk aquifer to the regional climatic signal. Journal of Hydrology 464-465, 485–493.
Farrant, A.R., Smart, P.L., 2011. Role of sediment in speleogenesis; sedimentation and paragenesis. Geomorphology 134, 79–93.
Farrant, A.R., Maurice, L., Ballesteros, D., Nehme, C., 2023. The genesis and evolution of karstic conduit systems in the Chalk. Geological Society of London, Special Publication 517, 1. https://doi.org/10.1144/SP517-2020-126.
Flipo, N., Gallois, N., Labarthe, B., Baratelli, F., Viennot, P., Schuite, J., Rivière, A., Bonnet, R., Boé, J., 2020. Pluri-annual water budget on the Seine Basin: past, current and future trends. In: Flipo, N., Labadie, P., Lestel, L. (Eds.), The Seine River Basin. Springer, Cham, pp. 59–90.
Foley, A., Worthington, S.R.H., 2023. Advances in conceptualizing transport in Chalk aquifers. Geological Society of London, Special Publication 517, 1. https://doi.org/10.1144/SP517-2020-173.
Fournier, M., Massei, N., Bakalowicz, M., Dussart-Baptista, L., Rodet, J., Dupont, J.P., 2007. Using turbidity dynamics and geochemical variability as a tool for understanding the behavior and vulnerability of a karst aquifer. Hydrogeology Journal 15, 689–704.
Fournier, M., Massei, N., Mahler, B.J., Bakalowicz, M., Dupont, J.P., 2008. Application of multivariate analysis to suspended matter particle size distribution in a karst aquifer. Hydrological Processes 22, 2337–2345.
Frisia, S., Borsato, A., Fairchild, I.J., McDermott, F., 2000. Calcite fabrics, growth mechanisms, and environments of formation in speleothems from the Italian Alps and Southwestern Ireland. Journal of Sedimentary Research 70, 1183–1196.
Genuite, K., Todisco, D., Nehme, C., Ballesteros, D., Mouralis, D., 2021. Morphological evolution of the middle and lower Seine valley (Normandy, France) during the Quaternary: morphometrical analysis of the paleo-meanders. Quaternaire 32, 203–220.
Ghasemizadeh, R., Hellweger, F., Butscher, C., Padilla, I., Vesper, D., Field, M., Alshawabkeh, A., 2008. Groundwater flow and transport modeling of karst aquifers, with particular reference to the North Coast Limestone aquifer system of Puerto Rico. Hydrogeology Journal 20, 1441–1461.
Goeppert, N., Goldscheider, N., 2019. Improved understanding of particle transport in karst groundwater using natural sediments as tracers. Water Research 166, 115045. https://doi.org/10.1016/j.watres.2019.115045.
Goldberg, P., Sherwood, S.C., 2006. Deciphering human prehistory through the geoarcheological study of cave sediments. Evolutionary Anthropology: Issues, News, and Reviews: Issues, News, and Reviews 15, 20–36.
González-Lemos, S., Jiménez-Sánchez, M., Stoll, H.M., 2014. Sediment transport during recent cave flooding events and characterization of speleothem archives of past flooding. Geomorphology 228, 87–100.
Graham, A.G.C., Stoker, M.S., Lonergan, L., Bradwell, T., Stewart, M.A., 2011. The Pleistocene glaciation of the North Sea basin. In: Elhers, J., Gibbard, P.L. (Eds.), Quaternary Glaciations — Extent and Chronology. A Closer Look: Developments in Quaternary Science. Elsevier, Amsterdam, pp. 261–278.
Grube, A., Grube, F., Rickert, B.H., Strahl, J., 2017. Eemian fossil caves and other karst structures in cretaceous chalk and succeeding quaternary sediments covering the salt structure Krempe-Lägerdorf (SW Schleswig-Holstein, North Germany). Zeitschrift der Deutschen Gesellschaft für Geowissenschaften 168, 263–284.
Guilloré, P., 1980. Méthode de fabrication mécanique et en série des lames minces. Institut National d'Agronomie, Paris-Grignon (22 pp.).
Hakoun, V., Orban, P., Dassargues, A., Brouyère, S., 2017. Factors controlling spatial and temporal patterns of multiple pesticide compounds in groundwater (Hesbaye chalk aquifer, Belgium). Environmental Pollution 223, 185–199.
Harmand, D., Adamson, K., Rixhon, G., Jaillet, S., Losson, B., Devos, A., Hez, G., Calvet, M., Audra, P., 2017. Relationships between fluvial evolution and karstification related to climatic, tectonic and eustatic forcing in temperate regions. Quaternary Science Reviews 166, 38–56.
Häuselmann, A.D., Häuselmann, P., Onac, B.P., 2010. Speleogenesis and deposition of sediments in Cioclovina Uscata Cave, Sureanu Mountains, Romania. Environment and Earth Science 61, 1561–1571.
Heiss, J., Condon, D.J., McLean, N., Noble, S.R., 2012. 238U/235U systematics in terrestrial uranium-bearing minerals. Science 335, 1610–1614.
Hellstrom, J., 2006. U-Th dating of speleothems with high initial 230Th using stratigraphical constraint. Quaternary Geochronology 1, 289–295.
Herman, E.K., Toran, L., White, W.B., 2008. Threshold events in spring discharge: evidence from sediment and continuous water level measurement. Journal of Hydrology 351, 98–106.
Herman, E.K., Toran, L., White, W.B., 2012. Clastic sediment transport and storage in fluviokarst aquifers: an essential component of karst hydrogeology. Carbonates and Evaporites 27, 211–241.
House, A.R., Thompson, J.R., Sorensen, J.P.R., Roberts, C., Acreman, M.C., 2016. Modelling groundwater/surface water interaction in a managed Riparian Chalk Valley Wetland. Hydrological Processes 30, 447–462.
Kurečić, T., Bočić, N., Wacha, L., Bakrač, K., Grizelj, A., Tresić Pavičić, D., Lüthgens, C., Sironić, A., Radović, S., Redovniković, L., Fiebig, M., 2021. Changes in cave sedimentation mechanisms during the late Quaternary: an example from the Lower Cerovačka Cave, Croatia. Frontiers in Earth Science 9. https://doi.org/10.3389/feart.2021.672229.
Laignel, B., Quesnel, F., Meyer, R., Macaire, J.J., 1998. Relations quantitatives entre les craies à silex et les formations résiduelles à silex de l'ouest du bassin de paris. Geodinamica Acta 11, 171–181.
Laignel, B., Spencer, C.H., Meyer, R., 2002. The clay-with-flints of the western Paris Basin: a potential aggregate resource. Environmental Geology 41, 525–536.
Laignel, B., Quesnel, F., Spencer, C., Meyer, R., Lautridou, P., 2003. Slope clay-with-flints (biefs à silex) as indicators of Quaternary periglacial dynamics in the western part of the Paris Basin, France. Journal of Quaternary Science 18, 295–299.

Laignel, B., Dupuis, E., Rodet, J., Lacroix, M., Masséi, N., 2004. An example of sedimentary filling in the chalk karst of the Western Paris Basin characterization, origins and hydrosedimentary behaviour. Zeitschrift für Geomorphologie 48, 219–243.
Lambeck, K., 1997. Sea-level change along the French Atlantic and Channel coasts since the time of the Last Glacial Maximum. Palaeogeography Palaeoclimatology Palaeoecology 129, 1–22.
Lamont-Black, J., Mortimore, R., 2000. Dissolution tubules: a new structure from the English Chalk. Zeitschrift für Geomorphologie 44, 469–489.
Lanos, P., Dufresne, P., 2019. ChronoModel version 2.0: software for chronological modelling of archaeological data using Bayesian statistics. https://chronomodel.com/. (Accessed 1 December 2022).
Lanos, P., Philippe, A., 2018. Event date model: a robust Bayesian tool for chronology building. Communications for Statistical Methods and Applications 25, 131–157.
Lasseur, E., Guillocheau, F., Robin, C., Hanot, F., Vaslet, D., Coueffe, R., Neraudeau, D., 2009. A relative water-depth model for the Normandy Chalk (Cenomanian-Middle Coniacian, Paris Basin, France) based on facies patterns of metre-scale cycles. Sedimentary Geology 213, 1–26.
Lautridou, J.P., Baize, S., Clet, M., Coutard, J.P., Ozouf, J.C., 1999. Les séquences plio-pléistocènes littorales et estuariennes de Normandie [Littoral and estuarine Plio-Pleistocene sequences in Normandy (France)]. Quaternaire 10, 161–169.
Lolcama, J.L., Cohen, H.A., Tonkin, M.J., 2002. Deep karst conduits, flooding, and sinkholes: lessons for the aggregates industry. Engineering Geology 65, 151–157.
Lundberg, J., McFarlane, D.A., 2007. Pleistocene depositional history in a periglacial terrane: a 500 k.y. record from Kents Cavern, Devon, United Kingdom. Geosphere 3, 199–219.
Mahler, B.J., Personné, J.C., Lods, G.F., Drogue, C., 2000. Transport of free and particulate-associated bacteria in karst. Journal of Hydrology 238, 179–193.
Martini, I., 2011. Cave clastic sediments and implications for speleogenesis: new insights from the Mugnano Cave (Montagnola Senese, Northern Apennines, Italy). Geomorphology 134, 452–460.
Martini, I., Ronchitelli, A., Arrighi, S., Capecchi, G., Ricci, S., Scaramucci, S., Spagnolo, V., Gambassini, P., Moroni, A., 2018. Cave clastic sediments as a tool for refining the study of human occupation of prehistoric sites: insights from the cave site of La Cala (Cilento, southern Italy). Journal of Quaternary Science 33, 586–596.
Massei, N., Wang, H.Q., Dupont, J.P., Rodet, J., Laignel, B., 2003. Assessment of direct transfer and resuspension of particles during turbid floods at a karstic spring. Journal of Hydrology 275, 109–121.
Maurice, L.D., Atkinson, T.C., Barker, J., Williams, A.T., Gallagher, A., 2012. The nature and distribution of flowing features in a weakly karstified porous limestone aquifer. Journal of Hydrology 438-439, 3–15.
Maurice, L., Farrant, A.R., Mathewson, E., Atkinson, T., 2023. Karst hydrogeology of the Chalk and implications for groundwater protection. Geological Society of London, Special Publication 517, 1. https://doi.org/10.1144/sp517-2020-267.
Mellett, C.L., Hodgson, D.M., Plater, A.J., Mauz, B., Selby, I., Lang, A., 2013. Denudation of the continental shelf between Britain and France at the glacial-interglacial timescale. Geomorphology 203, 79–96.
Miller, C.R., James, N.P., Bone, Y., 2012. Prolonged carbonate diagenesis under an evolving late cenozoic climate; Nullarbor Plain, southern Australia. Sedimentary Geology 261-262, 33–49.
Mortimore, R.N., 2019. Late Cretaceous to Miocene and Quaternary deformation history of the Chalk: Channels, slumps, faults, folds and glacitectonics. Proceedings of Geological Association 130, 27–65.
Mortimore, R., Newman, T.G., Royse, K., Scholes, H., Lawrence, U., 2011. Chalk: its stratigraphy, structure and engineering geology in East London and the Thames Gateway. Quarterly Journal of Engineering Geology & Hydrogeology 44, 419–444.
Murphy, P., Westerman, A.R., Clark, R., Booth, A., Parr, A., 2008. Enhancing understanding of breakdown and collapse in the Yorkshire Dales using ground penetrating radar on cave sediments. Engendering Geology 99, 160–168.
Murszewski, A., Boschian, G., Herries, A.I.R., 2020. Complexities of assessing palaeocave stratigraphy: Reconstructing site formation of the ~2.61 Ma Drimolen Makondo fossil site. PeerJ 8. https://doi.org/10.7717/peerj.10360.
Murton, J.B., Belshaw, R.K., 2011. A conceptual model of valley incision, planation and terrace formation during cold and arid permafrost conditions of Pleistocene southern England. Quaternary Research 75, 385–394.
Nehme, C., Farrant, A., Ballesteros, D., Todisco, D., Rodet, J., Sahy, D., Grappone, J.M., Staigre, J., Mouralis, D., 2020. Reconstructing fluvial incision rates based upon palaeo-water tables in Chalk karst networks along the Seine valley (Normandy, France). Earth Surface Processes and Landforms 45, 1860–1876.
Nobre, J.A., Freire, A.F.M., Neto, A.A., dos Santos Martins, M., Silva, C.G., Vieira, R., 2020. Quaternary warming and cooling trends in the Bransfield Basin, Antarctic Peninsula, based on gamma-ray spectrometry. Geo-Marine Letters 40, 781–788.
North American Commission on Stratigraphic Nomenclature, 1983. North American Stratigraphic Code. American Association of Petroleum Geologists Bulletin 67, 841–875.
Piccini, L., 2011. Speleogenesis in highly geodynamic contexts: the Quaternary evolution of Monte Corchia multi-level karst system (Alpi Apuane, Italy). Geomorphology 134, 49–61.
Price, M., Downing, R.A., Edmunds, W.M., 1993. The Chalk as an aquifer. In: Downing, R.A., Price, M., Jones, G.P. (Eds.), The Hydrogeology of the Chalk of North-West Europe. Clarendon Press, Oxford, pp. 14–34.
Proctor, C.J., Berridge, P.J., Bishop, M.J., Richards, D.A., Smart, P.L., 2005. Age of Middle Pleistocene Fauna and Lower Palaeolithic Industries from Kent's Cavern, Devon. Quaternary Science Reviews 24, 1243–1252.
Quesnel, F., Catt, J., Laignel, B., Bourdillon, C., Meyer, R., 2003. The Neogene and Quaternary Clay-with-flints north and south of the English Channel: comparisons of distribution, age, genetic processes and geodynamics. Journal of Quaternary Science 18, 283–294.
Reeve, T., 2021. Caves in the Chalk: a personal perspective from 50 years of observations. Cave and Karst Science 48, 43–55.
Reinhardt, N., Herrmann, L., 2018. Gamma-ray spectrometry as versatile tool in soil science: a critical review. Journal of Plant Nutrition and Soil Science 182, 9–27.
Richard, M., Pons-Branchu, E., Genuite, K., Jaillet, S., Joannes-Boyau, R., Wang, N., Genty, D., Cheng, H., Price, G.J., Pierre, M., Dapoigny, A., Falguères, C., Tombret, O., Voinchet, P., Bahain, J.J., Moncel, M.H., 2021. Timing of Neanderthal occupations in the southeastern margins of the Massif Central (France): a multi-method approach. Quaternary Science Reviews 273, 107241. https://doi.org/10.1016/j.quascirev.2021.107241.
Robert, T., Dassargues, A., Brouyère, S., Kaufmann, O., Hallet, V., Nguyen, F., 2011. Assessing the contribution of electrical resistivity tomography (ERT) and self-potential (SP) methods for a water well drilling program in fractured/karstified limestones. Journal of Applied Geophysics 75, 42–53.
Rodet, J., 2013. Karst et évolution géomorphologique de la côte crayeuse à falaises de la manche. L'exemple du massif d'Aval (Étretat, Normandie, France). Quaternaire 24, 303–314.
Rodet, J., Lautridou, J.P., 2003. Contrôle du karst quaternaire sur la genèse et l'évolution du trait de côte d'une région crayeuse de la Manche (Pays de Caux, Normandie, France). Quaternaire 14, 31–42.
Rodet, J., Laignel, B., Brocard, G., Dupuis, E., Massei, N., Viard, J.P., 2006. Contribution of a sedimentary study to the karstic evolution concept of a chalk cave of the Western Paris Basin (Normandy, France). Geologica Belgica 9, 287–296.
Rohling, E.J., Yu, J., Heslop, D., Foster, G.L., Opdyke, B., Roberts, A.P., 2021. Sea level and deep-sea temperature reconstructions suggest quasi-stable states and critical transitions over the past 40 million years. Science Advancs 7, 1–18.
Roux, J.C., Gaillard, T., Hauchard, E., 2019. Le système hydrogéologique karstique crayeux des sources d'Yport (Seine-Maritime). Évolution des connaissances et exploitation de la ressource. Géologues 199, 73–82.
Sanz, E., Rosas, P., Menéndez-Pidal, I., 2016. Drainage and siphoning of a karstic spring: a case study. Journal of Cave Karst Studies 78, 183–197.
Schiperski, F., Zirlewagen, J., Scheytt, T., 2016. Transport and attenuation of particles of different density and surface charge: a karst aquifer field study. Environmental Science & Technology 50, 8028–8035.
Sharp, J.M., Green, R.T., Schindel, G.M., 2019. The Edwards Aquifer: The Past, Present, and Future of a Vital Water Resource. Geological Society of America, Boulder.
Singer, A., 1984. The paleoclimatic interpretation of clay minerals in sediments - a review. Earth-Science Reviews 21, 251–293.
Stenestad, E., 2006. Fluviokarst in the top of the Maastrichtian chalk at Rørdal, Northern Jut-land, Denmark. Bulletin of the Geological Society of Denmark 53, 93–110.
Tourenq, J., Pomerol, C., 1995. Mise en évidence, par la présence d'augite du Massif Central, de l'existence d'une pré Loire- pré Seine coulant vers la Manche au Pléistocène. Comptes Rendus de l'Académie des Sciences 320, 1163–1169.
Van Lint, J., Giot, D., Callec, Y., 2003. Carte géologique harmonisée du département de l'Eure. Bureau de Recherches Géologiques et Minières, Paris (97 pp.).
Veni, G., 2013. A framework for assessing the role of karst conduit morphology, hydrology, and evolution in the transport and storage of carbon and associated sediments. Acta Carsologica 42, 203–211.
Vesper, D.J., Loop, C.M., White, W.B., 2001. Contaminant transport in karst aquifers. Theoretical and Applied Karstology 13-14, 101–111.
Waltham, A.C., Fookes, P.G., 2003. Engineering classification of karst ground conditions. Quarterly Journal of Engineering Geology & Hydrogeology 36, 101–118.
Warren, C.D., Mortimore, R.N., 2003. Chalk engineering geology - Channel Tunnel Rail Link and North Downs Tunnel. Quarterly Journal of Engineering Geology & Hydrogeology 36, 17–34.
Westaway, R., 2004. Pliocene and Quaternary surface uplift evidenced by sediments of the Loire Allier river system (France). Quaternaire 15, 103–115.
Wetherell, A., 2023. Rivers, streams and wetlands – the Chalk and its water dependant ecosystems. Geological Society of London, Special Publication 517, 1. https://doi.org/10.1144/sp517-2020-140.
White, W.B., 2007. Cave sediments and paleoclimate. Journal of Cave Karst Studies 69, 76–93.
Willems, L., Rodet, J., Fournier, M., Laignel, B., Dusar, M., Lagrou, D., Pouclet, A., Massei, N., Dussart-Baptista, L., Compère, P., Ek, C., 2007. Polyphase karst system in Cretaceous chalk and calcarenite of the Belgian-Dutch border. Zeitschrift für Geomorphologie 51, 361–376.